# DISTRIBUTION SYSTEM PERFORMANCE IMPROVEMENT USING META-HEURISTIC OPTIMIZATION ALGORITHMS

by

**Hasan Jamil Apon (170021073)**
**Khandaker Adil Morshed (170021087)**
**Md. Shadman Abid (170021093)**

A Thesis Submitted to the Academic Faculty in Partial Fulfillment of the Requirements for the Degree of

## BACHELOR OF SCIENCE IN ELECTRICAL AND ELECTRONIC ENGINEERING

Department of Electrical and Electronic Engineering
**Islamic University of Technology (IUT)**
Gazipur, Bangladesh

# DISTRIBUTION SYSTEM PERFORMANCE IMPROVEMENT USING META-HEURISTIC OPTIMIZATION ALGORITHMS

Approved by:

------------------------------------------
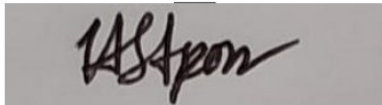
**Dr. Ashik Ahmed**

Supervisor and Professor,
Department of Electrical and Electronic Engineering,
Islamic University of Technology (IUT),
Boardbazar, Gazipur-1704.

Date: ..10/5/22

# Declaration of Authorship

This is to certify that the work presented in this thesis paper is the outcome of research carried out by the candidates under the supervision of Dr. Ashik Ahmed, Professor, Department of Electrical and Electronic Engineering (EEE), Islamic University of Technology (IUT).
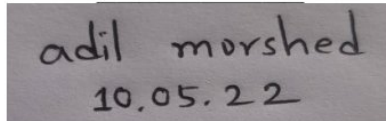
## Authors

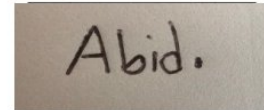**Hasan Jamil Apon**

ID: 170021073

**Khandaker Adil Morshed**

ID: 170021087

**Md. Shadman Abid**

ID: 170021093

# Contents

# List of Figures

# List of Tables

# Abstract

The critical challenge for an efficient islanding operation of a distribution system having Distributed Generation (DG) is preserving the frequency and voltage stability. Contemporary load shedding schemes are inefficient and do not adequately assess the optimum amount of load to shed which results in either excessive or inadequate load shedding. Appropriate installation of renewable energy-based distributed generation units (RDGs) is one of the most important challenges and current topics of interest in the optimal functioning of modern power networks. Due to the intermittent nature of renewable energy sources, optimal allocation and sizing of RDGs, particularly photovoltaic (PV) and wind turbine (WT), remains a critical task. Additionally, maintaining frequency and voltage stability is crucial for optimal functioning of an islanded network connected to DGs. Conventional load shedding schemes do not effectively identify the optimal amount of load to shed, culminating in either excessive or insufficient load shedding. Hence, the first part of this work presents an optimal load shedding technique using Chaotic Slime Mould Algorithm (CSMA) with sinusoidal map in order to achieve greater efficiency. A constrained function with static voltage stability margin (VSM) index and total remaining load after load shedding was applied to accomplish the evaluation. A total of three islanding scenarios of IEEE 33 bus and IEEE 69 bus radial distribution systems were used as test systems to assess the efficacy of the proposed load shedding approach using MATLAB software. To identify performance enhancements, the developed method was compared to Backtrack Search Algorithm (BSA) and the original SMA. According to the results, CSMA outperforms both BSA and SMA in terms of remaining load and voltage stability margin index values in all the test systems. Moreover, the second part of this work proposes Chaotic Equilibrium Optimizer (CEO) with iterative map to achieve an optimal solution for multiple DG sizing and placement in distribution networks, as well as an optimal load shedding approach. Regarding DG placement, the objective function was to minimize total active power loss and voltage deviation of the network nodes. The proposed method was compared with Modified moth flame optimization (MMFO), Teaching learning based optimization (TLBO) and the original Equilibrium optimizer (EO). Moreover, to assess the optimal load shedding technique, a constrained function with total remaining load and static voltage stability margin (VSM) index was used. In addition, the proposed CEO algorithm is compared with some of the recent metaheuristics algorithms applied in this domain such as Grasshopper optimization algorithm (GOA), Backtrack search algorithm (BSA) and the original Equilibrium optimizer (EO). In the last part of the work, based on a new metaheuristic known as the Artificial hummingbird algorithm (AHA), this work provides a novel approach for addressing the problem of RDG planning optimization. Considering various operational constraints, the optimization problem is developed with multiple objectives

including power loss reduction, voltage stability margin (VSM) enhancement, voltage deviation minimization, and yearly economic savings. Furthermore, using relevant probability distribution functions, the ambiguities related with the stochastic nature of PV and WT output powers are evaluated. The proposed algorithm was compared to two of the recent metaheuristics applied in this domain known as improved harris hawks and particle swarm optimization algorithm (HHO-PSO) and hybrid of phasor particle swarm and gravitational search algorithm (PPSOGSA). The IEEE 33-bus and 69-bus systems are assessed as the test systems in this study. According to the findings, AHA delivers superior solutions and enhances the techno-economic benefits of distribution systems in all the scenarios evaluated.

# Chapter 1

## 1 Introduction

## 1.1 Optimal Load-Shedding in Distribution System

Due to increasing load uncertainties and multiple DGs including renewable energy sources, one of the vital issues of contemporary power networks is appropriate load shedding (LS) scheme as a contingency plan. Under frequency load shedding (UFLS) and under voltage load shedding (UVLS), two significant LS strategies that leverage frequency and voltage stability as determining factors for balanced functioning of an electrical system are frequently employed for analysis purposes[1]. Steady state voltage instability is generally caused by overloading of the network nodes or an accidental interruption of a cable or power source, which can lead to increased reactive power demand and subsequently a blackout. Moreover, steady state voltage stability indicates the ability of the system to thrive with balanced voltages at all the nodes when the network is subjected to a substantial disturbance under typical operating conditions. UVLS is the most appropriate countermeasure for avoiding voltage collapse if the fault could be foreseen and only implemented as a last alternative in severe circumstances to avert a high-scaled voltage breakdowns [2]. Therefore, UVLS strategy formulation is essential to recognize appropriate load shedding techniques in order to prevent system voltage collapsing, which is a crucial objective in the development of such defense mechanisms. Additionally, numerous operational constraints emerges in a DG integrated distribution system if the utility supply is interrupted and the system becomes islanded. Among these operational constraints, sustaining the voltage stability of the islanded system is the most significant issue and load shedding is regarded as the most efficient method of addressing the challenge.

Numerous works have suggested several optimum load-shedding strategies using conventional optimization algorithms and machine learning approaches including artificial neural network (ANN), deep reinforcement learning, fuzzy logic, etc to accomplish the most stable operating point for electrical networks with the least amount of load curtailment while fulfilling suitable criteria [3-10]. To illustrate further, the authors in [11] suggested a novel technique employing genetic algorithm (GA) to address the steady state load-shedding phenomenon in distribution networks with DG during generation shortage scenarios, with the objective of minimizing total curtailed load and system losses. Moreover, the work in [12] proposed an adaptive strategy in which the frequency of the system after a disruption is anticipated using the particle swarm optimization (PSO)

algorithm. Consequently, the amount of load that must be shed in order to keep the frequency of the system within the allowable limits is identified. In addition, M.Talaat et al. introduced grasshopper optimization algorithm (GOA) approach in order to reduce the amount of load shed while maximizing the lowest swing frequency [13]. Furthermore, the work in [14] exhibited the efficiency of a bacterial foraging optimization algorithm (BFOA) in an electrical network for optimum load shedding, with the fitness function defined by total power losses and voltage stability index. Moreover, differential evolution (DE) algorithm, which takes into consideration inequality constraints not only on the current operating condition, but also in the forecasted next sequence load, was used for instantaneous load shedding to ensure precise load shedding at selected buses under emergency circumstances in order to prevent voltage instability. The locations for load curtailment were selected depending on the intensity of the load flow's smallest eigenvalue to load restriction [15]. Additionally, the significance of demand prioritization on power system operation during emergencies was studied to justify the alliance algorithm's substantial benefits over current heuristic approaches in steady-state load-shedding[16]. Besides, an UVLS optimization technique termed as evolutionary particle swarm optimization (EPSO) was adopted in order to identify the best remaining load quantity while reducing power loss, voltage variation, and load shedding cost [17]. In addition, the study in [18] was focused on the development of an efficient load shedding technique in an islanded distribution network using BSA.

The optimal UVLS method is a complicated non-linear approach and finding a globally optimal solution in a vast solution space is a difficult undertaking because it necessitates a resilient and widely applicable optimization technique. The significance of optimization in this domain cannot be overstated, as it would be advantageous if additional load could be provided with the assistance of a novel or modified optimization method that also assures a better voltage profile of the system. Hence, the objective of this work is to focus on improving under-voltage load shedding schemes by maintaining the system's maximum possible load while ensuring voltage stability. In this context, sinusoidal chaos has been integrated with a recently developed meta-heuristic algorithm known as Slime Mould Algorithm (SMA) in order to explore performance enhancement. The suggested SMA approach includes an atypical mathematical model with dynamic weights that replicates bipolar feedback of the dispersion wave of the slime moulds in order to identify the optimum path for adhering food with a high exploitation potential and exploratory aptitude. In addition, integrating the sinusoidal chaos with SMA can vastly enhance search speed and efficiency. Accordingly, the performance of the recommended chaotic slime mould algorithm (CSMA) is evaluated and its effectiveness over the original SMA and BSA [19] is verified by comprehensive statistical analysis.

## 1.2   Optimal Sizing and Placement of Multiple DG Units

The extensive use of fossil fuels, severe environmental implications, and increased transmission and distribution losses in traditional power networks have drawn attention to non-conventional energy sources. DGs are currently playing a key role in reducing power losses, enhancing voltage stability, and increasing dependability of power networks. However, unplanned and unregulated installation of DGs can cause major issues and challenges for power systems. These concerns include the likelihood of bidirectional power flow as well as the critical challenges including higher power losses, voltage drop, reactive power management and power quality issues. Furthermore, integrating DGs above a particular threshold has a detrimental impact on the overall power system protection mechanism [20]. Under voltage load shedding (UVLS) is one of the most important load shedding (LS) schemes that uses voltage stability as a determinant in the proper governing of an electrical network [21]. Besides, under normal operating conditions, voltage stability signifies the network's capability to maintain balanced voltages when the system experiences a major disruption. Furthermore, if the power source is interrupted and the network becomes islanded, distribution network encounters a number of operating restrictions. Among these restrictions, the fundamental problem is maintaining the voltage stability and UVLS is recognized as the feasible mitigation strategy for avoiding high-scaled voltage breakdowns [22].

Numerous studies have been conducted in recent years to determine the best techniques for allocating DGs in the most efficient manner with varying types, sizes, and numbers of DGs. The studies suggested in [23-26] directs researchers and power system engineers to various methodologies and models for systematically and qualitatively assessing the best distributed generation (DG) deployment in power distribution networks. To illustrate, particle swarm optimization (PSO) was proposed by the authors of [26] for optimum deployment of various types of DG sources in power systems with the objective of lowering total energy loss. Moreover, to allocate DGs in the most optimum locations, [27] suggested a hybrid grey wolf optimizer, which is a hybrid meta-heuristic algorithm. This article found the placement of the DGs by reducing total actual power loss while maintaining certain constraints. The authors of [28] introduced fuzzy logic controller (FLC) approaches and the ant-lion optimization algorithm (ALOA) paired with particle swarm optimization (PSO) in order to assign multi-DGs at different sites to provide an optimum solution. Furthermore, properly sized DG units were installed at optimal locations in the works of[29] by utilizing a chaotic differential evolution approach by considering power loss, annual economic loss, and voltage deviation as multi-objective fitness function. The authors of [30] offer a modified Moth Flame Optimization approach for determining the best position and size of DGs by minimizing running costs while also minimizing total active power and voltage deviation. The

3

authors of the work [31] developed a decision-making technique for the challenge of optimum size and location of DG units. The method is centered on improving voltage profiles and lowering overall real and reactive power losses. Additionally, binary particle swarm optimization suggested in [32] results in optimal configuration of multiple DG units by placing DGs in suitable places to reduce power loss and enhance voltage profiles. The research in [33] provides an analytical index for optimizing the appropriate size and placement of DG based on loss sensitivity factor, voltage stability margin, and reliability based parameters. To decrease distribution system losses, [34] proposed a hybrid approach combining the grasshopper optimization algorithm (GOA) and the cuckoo search (CS) technique to identify the position and size of DGs. [35] offers a multi-objective system that employs binary particle swarm optimization and shuffled frog leap algorithms (BPSO-SLFA) to determine the appropriate size and position of DG in order to improve voltage profiles by decreasing power losses. Furthermore, the study in [36] provides an enhanced Harris Hawks Optimizer for determining optimal placement of DG at various operational power factors in order to decrease active power loss and voltage deviation.

Similarly, several studies have proposed various optimal load-shedding techniques based on traditional optimization algorithms and machine learning algorithms. [37] presents an load shedding method based on the grasshopper optimization algorithm (GOA) that reduces the amount of load to be shed while maintaining highest swing frequency possible at all phases. [38] introduces a constrained multi-objective function that integrates the voltage stability margin index with the amount of load curtailment. This objective function was optimized by employing an optimum load shedding technique based on the backtrack search algorithm (BSA). Furthermore, to avoid voltage instability, the differential evolution (DE) algorithm was utilized for instantaneous load shedding at particular nodes [39]. The study in [40] proposes bacterial foraging optimization algorithm (BFAO) for optimal load shedding by reducing total power loss and total costs as well as improving the stability of system. In addition, in order to show the alliance algorithm's benefits in typical load-shedding, the influence of load precedence on electrical system performance during emergencies was investigated [41]. Moreover, an optimal approach termed as evolutionary particle swarm optimization (EPSO) is used in [42] to find the suitable residual load while lowering voltage fluctuation, energy losses, and load shedding expense.

The aforementioned works reveal that both the optimal DG placement as well as optimum load shedding for distribution systems are continuous challenges. The implication of optimization approaches in this research domain cannot be overstated, since it would be beneficial if substantial improvements could be accomplished using an unique or updated optimization methodology that also enhances the network's voltage profile. Hence, the objectives of this work are identified

as follows. **Firstly, appropriate placement and sizing of DGs with the objective of minimizing active power loss and preserving system voltage stability. Secondly, the emphasis was on enhancing the UVLS scheme by keeping the system at its maximum feasible load while assuring voltage stability.** In this regard, this study adopts a recently developed algorithm called Equilibrium Optimizer (EO) and modifies it with the incorporation of iterative map in order to identify the optimal solution with high exploitation potential and exploratory aptitude. The algorithm is based on dynamic source and sink frameworks based on physics, which are utilized to generate equilibrium states derived from natural mathematical concepts. Moreover, combining iterative chaos with EO can significantly improve efficiency and search speed. The proposed chaotic equilibrium optimizer's (CEO) performance is evaluated, and its superiority over Teaching Learning Based Optimization (TLBO) [43], modified Moth Flame Optimization (MMFO) , and Equilibrium Optimizer (EO) is validated through extensive statistical analysis for optimal DGs sizing and placement. Furthermore, for optimal load shedding optimization, the performance of the proposed CEO is investigated, and its efficiency is compared with some of the recent metaheuristics algorithms applied in this domain such as GOA ,BSA[44] , and EO. The IEEE 33-bus and 69-bus systems are assessed as the test systems in this study.

## 1.3 Optimal Planning of Multiple Renewable Energy-Integrated Distribution System with Uncertainties

The demand for electricity is increasing all around the world due to advancements in science and technology. The existence of industrial activities and social structures relies mostly on low cost and uninterrupted supply of electrical energy [45]. Although fossil fuels are the primary source of power generation, their resources are rapidly depleting, putting the future of fossil fuels in jeopardy. As a result, the current tendency is to use renewable energy sources such as solar energy, wind energy, water energy, and nuclear energy to generate electricity. Optimal integration and planning of RDG unit installation (such as WTs and PVs) in distribution networks can be a feasible solution to the difficulties associated with conventional energy source scarcity.

Various studies have been conducted over the years investigating the potential benefits, challenges and scopes of RDG implementation on distribution networks. For instance, the authors of [46] highlight the major concerns, possibilities, and constraints of integrating distributed generation into electric power networks. Renewable energy sources are now the most convenient and profitable source of DGs. Moreover, [47] depicts the future prospects and scientific developments to harness renewable energy sources. Various sources of renewable energy and their benefits, growth, investment and deployment have been illustrated. Along with these works, many of the studies like [48-51]

have explored the integration of renewable energy sources into electric power systems and smart power grids, taking into account the availability of renewable energy sources. RDGs are gaining attraction as a solution for high power demand to reduce dependency on diminishing coal, fossil fuels, and natural gas. For instance, the authors of [52] suggest a comprehensive review of grid-integrated DG planning. Additionally, depending on certain factors such as generator type, penetration level, and grid features, the influence of RDGs on the distribution grid has been demonstrated in [53]. It should be noted that electricity generated from renewable energy sources is heavily influenced by external factors such as temperature, weather, wind speed, and humidity. The work in [54] discusses the financial issues as well as the broader economic and societal effects of distributed energy generation. Besides, the authors of [55] explore the environmental advantages of dispersed energy resources and their influence on lowering greenhouse gas emissions. The authors of [56] established RDG planning and scheduling approach using uncertainty modeling methodologies to provide techno-economic and environmental benefits. Furthermore, [57] creates an efficient operational schedule for multi-grid distribution systems while taking into account the uncertain environment of energy storage systems. Moreover, the works in [58] present a planning framework to increase the resilience of power-water distribution networks, with the goal of lowering the investment costs associated with the suggested techniques. In order to optimize techno-economic benefits, the authors of [59] utilize an algorithm for optimum integration of DGs in active distribution system (ADS) networks.

The energy provided by RDG sources is heavily influenced by factors like weather, temperature, site location, and time. The primary research problem in this subject is to deal with uncertainty in DG integrated power system networks. Furthermore, unregulated and inappropriate RDG unit penetration in distribution networks may impair system performance. Several studies have been conducted in the field of optimal sizing and allocation or placement of multiple and multi-type DGs in distribution systems employing optimization techniques. For instance, [60] discusses some approaches which can handle uncertainties like monte carlo simulation (MCS), scenario-based analysis (SBA), point estimate method (PEM) etc. A monte carlo simulation (MCS) based probabilistic method has been designed in [61] to examine the impact of wind power and PV power generation on distribution networks. Besides, [62] takes the help of MCS and particle swarm optimization (PSO) for optimal sizing of renewable energy systems considering stochastic behaviour of energy resources. The authors in [63] proposed improved harris hawks based particle swarm optimizer (HHO-PSO) for integrating renewable energy sources into distribution networks incorporating PV and WT generation uncertainties. Furthermore, [64] suggests a hybrid mix of phasor particle swarm optimization and gravitational search algorithm (PPSOGSA) for integrating

renewable energy sources into distribution networks while accounting for PV and WT generation and load uncertainties. In [65], an optimization technique called ant lion optimization algorithm (ALOA) has been introduced for optimal sizing and allocation of RDGs in a radial distribution network. Besides, in many of the works [66-72], backtrack search optimization algorithm (BSOA), artificial bee colony (ABC) algorithm, hybrid grey wolf optimizer, bacterial foraging optimization algorithm (BFOA), intelligent water drop (IWD) algorithm, stud krill herd algorithm (SKHA), and combined genetic algorithm-particle swarm optimization (GA-PSO) algorithm techniques were proposed for optimal DG sizing and placement. Moreover, optimization methods like mixed-integer non-linear programming (MINLP), multi-objective opposition based chaotic differential evolution (MOCDE) and evolutionary programming (EP) based technique have been suggested for optimal placement and sizing of DGs aiming loss minimization, and other techno-economic benefits [73-75]. The research in [76] employs the diagonal band Copula and the sequential monte carlo approach to optimally locate stochastic RDGs in imbalanced distribution power networks. Besides, [77] proposes a weighted aggregation PSO approach for tackling the selection of solar and wind RDGs based on their stochastic nature. Furthermore, the authors presented a bi-level metaheuristic method in [78] to solve the complex modelling approach of renewable energy sources and EV management in order to accomplish autonomous microgrids. In addition, [79] proposes an optimization technique for determining the ideal placements and sizes of solar and wind generation systems while also managing EVs to assemble an autonomous microgrid. [80] presents quasi-reflection based slime mould algorithm (QRSMA) for solving optimal allocation and sizing problems of capacitors and distribution generations. Moreover, the authors in [81] have discussed optimal allocation of renewable distributed generation (RDG) into distribution systems considering seasonal uncertainties of solar-wind load demands. [82] proposes a new approach for optimal scheduling of renewable-based multi-energy microgrid (MEM) systems which focuses on robust optimization with flexible energy conversion and storage devices. A multi-objective probabilistic approach has been adopted in [83] for smart voltage control of wind-energy integrated systems. Furthermore, [84] presents comprehensive research on multi-objective optimization of multiple energy integrated stations for improving energy conversion and utilization efficiency.

The RDG planning research domain also includes realistic distribution networks that use real-time data. For instances, in the works of [85], the whale optimization technique (WOA) algorithm was evaluated on IEEE 15-bus, 33-bus, 69-bus, and actual distribution networks like 85-bus and 118-bus test systems to determine the optimal DG-units size. Furthermore, the authors of [86] introduced a robust and effective technique called hybrid particle swarm optimization combined with gravitational search algorithm (PSOGSA) and MMFO for determining the optimal

location and capacity of RDG units for minimizing system power losses and operating costs while improving voltage profile and voltage stability. For simulation purposes, MEDN 15-bus and Moscow 111-bus practical test scenarios were analyzed. Besides, the authors of [87] proposed the power voltage sensitivity constant (PVSC) as a solution to the RDG allocation problem. A new metric is also proposed, which takes into account the amount of DG penetration as well as the percentage decrease in real power losses. The suggested technique's findings have been validated on a conventional IEEE 33 bus system and a 130 bus actual distribution system in Jamawaramgarh, Jaipur. Additionally, the indicators of loss sensitivity factors and bus voltage magnitudes are included in [88] to construct a set of fuzzy expert rules for asserting the preliminary buses for distributed generator placement. The suggested backtracking search technique (BSA) approach enables the fuzzy decision-maker to select the best option among the pareto-optimal choices available. On 33- and 94-node radial distribution networks with varied situations, the key aspects of the BSA technique are evaluated. Moreover, in the works of [89], the efficacy of an appropriate control mechanism is demonstrated with case studies for deterministic RDG placement on base configurations of IEEE 30-bus and 57-bus systems utilizing the SHADE-EC algorithm. The SHADE-EC method is also used to solve the single-objective and multi-objective stochastic instances.

### 1.3.1  Problem statement

Uncontrolled and excessive RDG unit penetration in distribution networks can have a negative impact on system performance. The prospect of bidirectional power flow, as well as difficulties such as higher power losses, voltage drop, reactive power management, and power quality issues, are among these concerns. Therefore, integration of RDG units in distribution networks necessitates much attention and proper planning to ensure the performance of the electrical network, such as system reliability, power quality, total active power loss reduction, and economic efficiency can be met. Besides, the power generated from RDG sources is mostly dependent on uncertainties like weather, temperature, location of site and time. The key challenge is to cope with uncertainties in DG integrated power system networks. Several studies have been conducted in the field of optimal sizing and allocation or placement of multiple and multi-type DGs in distribution systems employing different optimization techniques. The majority of these works are aimed at improving the distribution network's technical parameters in terms of power loss reduction and voltage stability. Besides, the preceding studies indicate that determining the appropriate RDG location for distribution networks is a continuous challenge. The significance of optimization techniques in this research domain cannot be overestimated, as it would be advantageous if major improvements

could be achieved utilizing a novel or modified optimization technique.

Research gaps

Based on the aforementioned literature review, the following findings may be formed:

- Very limited works have been published on optimal RDG allocation and size when PV and WT generation uncertainties are combined with load uncertainties.

- The majority of previous studies have ignored the techno-economic assessment of the proposed techniques.

- The voltage stability margin index ($VSM_{sys}$) has yet to be investigated in this research domain.

- AHA is unexplored in the research domain of RDG sizing and allocation when load and generation uncertainties are considered.

Main Contribution

The objective of this research is to evaluate the location and sizing of RDGs in order to minimize active power loss, maximize system voltage stability margins, minimize voltage deviation, and maximize overall yearly energy savings costs. The following is a list of the current work's major contributions:

- PV and WT power generation, as well as load variation, are all factored into the RDG sizing and allocation problem.

- The stochastic characteristics are achieved by using appropriate probability density functions (PDFs).

- The Artificial hummingbird algorithm (AHA), a recently developed algorithm, is used to determine the optimal solution with high exploitation potential and exploration aptitude.

- The performance of the suggested AHA is assessed, and its superiority over two of the most recent metaheuristics used in this domain known as hybrid phasor particle swarm optimization and gravitational search algorithm (PPSOGSA) and improved harris hawks based particle swarm optimizer (HHO-PSO) is demonstrated.

- Several scenarios of PV and WT penetration are explored to test the algorithm's efficacy, including and excluding uncertainties.

- In all the scenarios evaluated, AHA provides superior solutions and improves the techno-economic aspects of distribution networks.

9

# Chapter 2

## 2 Optimization Algorithm

### 2.1 Optimal Load-Shedding in Distribution System

### 2.1.1 Slime Mould Algorithm

The slime mould algorithm (SMA) proposed in [**90**] is a new meta-heuristic method that is used in this study to optimize the total remaining load and voltage profiles of islanded DG integrated distribution networks during load shedding. The technique is based on the slime mould's inherent oscillation pattern of food accessing in regard to air fragrances. The flowchart of the algorithm is depicted in Figure 2.2. The first step of SMA, like other meta-heuristic optimizations, is to create a random population set. The procedure may be stated as follows:

$$X = rand(UB - LB) + LB \tag{1}$$

where $LB$ and $UB$ signifies the lower and upper limits of each parameter in the parameter set, and $rand$ represents uniform random numbers between [0,1]. The next step is to compute fitness for each of the parameter sets and update the initial locations $X_{initial}(j = 1, 2, \ldots, n)$.

$$S = fitness(X) \tag{2}$$

$$[Smellorder, Smellindex] = sort(S) \tag{3}$$

Slime mould is highly reliant on the biological oscillator's propagation wave to regulate cytoplasmic flow in veins, placing them in a better position for food acquisition. To simulate the variations in venous width of slime moulds, fine tuning parameters $\overrightarrow{W}, \overrightarrow{vb}$ and $\overrightarrow{vc}$ are employed to materialize the changes. $\overrightarrow{W}$ mimics the oscillation rate of slime mould near various food contents, allowing slime mould to pursue food more rapidly when they find higher quality food, hence enhancing slime mould's efficiency in discovering the optimal sources of food. The weight of the food concentration $\overrightarrow{W}$ is denoted by the following expression:

$$\overrightarrow{W(smellindex(l))} = \begin{cases} 1 + rand * log(\frac{BF - S(j)}{BF - WF} + 1), & condition \\ 1 - rand * log(\frac{BF - S(j)}{BF - WF} + 1), & others \end{cases} \tag{4}$$
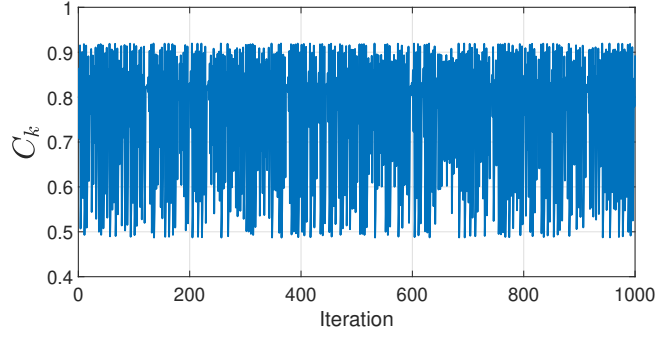
Figure 2.1: Chaotic sinusoidal map

where, $BF$ is the best fitness value achieved so far and $WF$ is the worst fitness value acquired in the current iteration. Eq.(4) analytically replicates the bipolar feedback between the vein thickness of the slime mould and the meal intake, where *condition* denotes that $S(j)$ belongs to the weights of the top half of the population. When the food concentration is increased, the region's weight begins to grow; when the food level is low, the region's weight reduces, leading to the exploration of other regions. The synergistic interplay of the other two fine-tuning factors, $\overrightarrow{vb}$ and $\overrightarrow{vc}$, mirrors slime mould's food selecting behavior. The formula for $\overrightarrow{vb}$ and $\overrightarrow{vc}$ is mentioned as follows:

$$\overrightarrow{vb} = [-a, a] \tag{5}$$

$$a = arctan(1 - \frac{t}{max\_t}) \tag{6}$$

$$\overrightarrow{vc} = [-b, b] \tag{7}$$

$$b = (1 - \frac{t}{max\_t}) \tag{8}$$

The array of $\overrightarrow{vb}$ is uniformly distributed randomly between $[-a, a]$ and gradually approaches zero as the number of iterations increases. The value of $\overrightarrow{vc}$ is also uniformly distributed between $[-1, 1]$ and consequently reaches zero. Slime mould determining whether to pursue the food source or seek alternative food sources is simulated by the uniform distribution of $\overrightarrow{vb}$. The location updating parameter $p$ is used to boost SMA's flexibility in various search phases, which increases the algorithm's versatility. .

$$p = tanhS(j) - DF \tag{9}$$

11
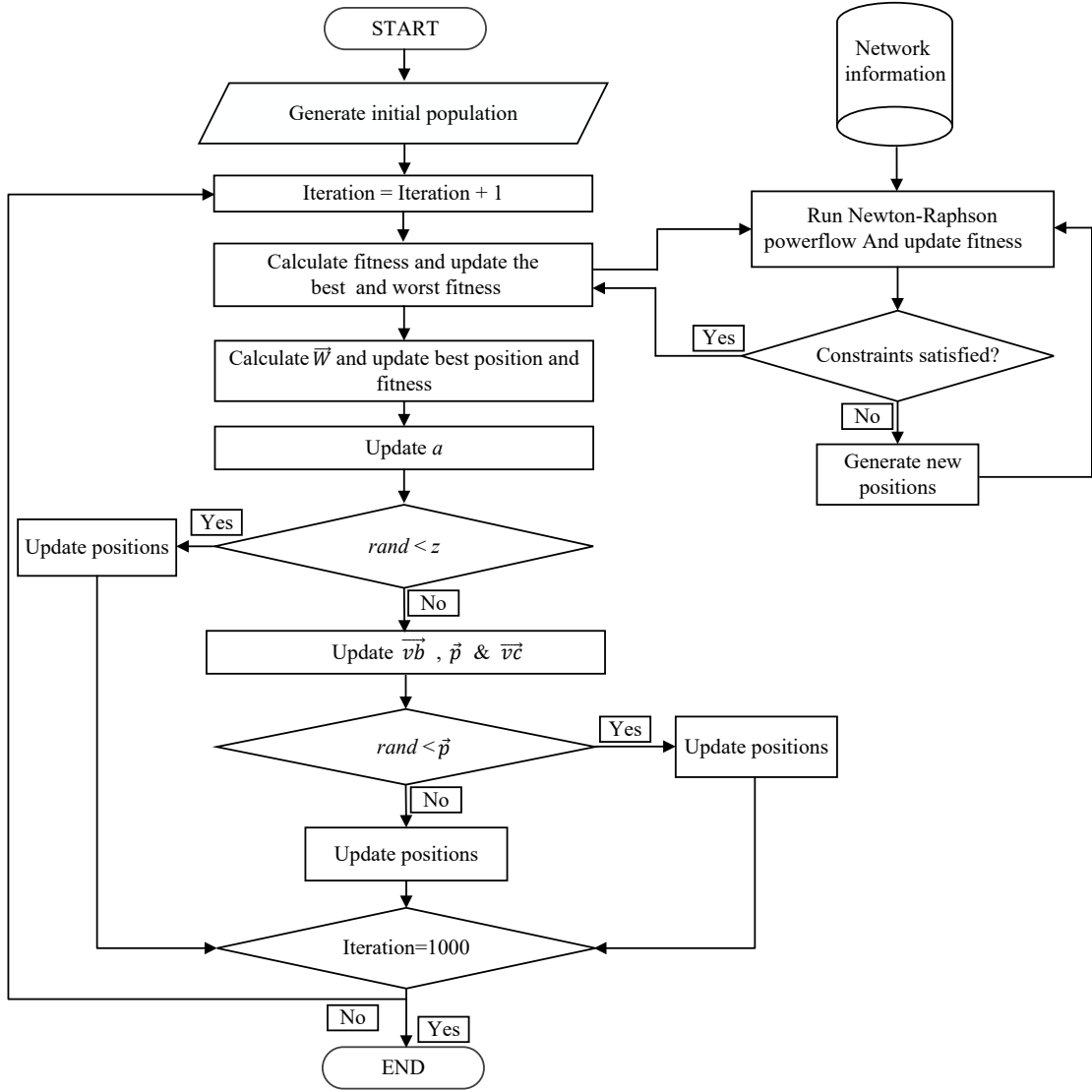
Figure 2.2: Slime mould algorithm

where $j = 1, 2, ..., n$, $S(j)$ reflects $X$'s fitness, and $DF$ represents the highest fitness acquired across all iterations. To emulate the whole contraction mode which was inspired by the dispersion and foraging behavior of slime mould, the following equation reflects its food approaching behavior:

$$\overrightarrow{X(t+1)} = \begin{cases} rand.(UB - LB) + LB, & rand < z \\ \overrightarrow{X_b}(t) + \overrightarrow{vb}.(\overrightarrow{W}.\overrightarrow{X_A(t)} - \overrightarrow{X_B(t)}), & rand < p \\ \overrightarrow{vc}.\overrightarrow{X(t)}, & rand \geq p \end{cases} \tag{10}$$

Where, $t$ denotes the immediate iteration, $\overrightarrow{X_b}$ represents the position with the highest smell concentration in immediate iteration, $\overrightarrow{X}$ represents slime mould position, $\overrightarrow{X_A}$ and $\overrightarrow{X_B}$ symbolize

two positions chosen at random from the slime mould and the value of $z$ is kept constant as 0.03 as the probability keeps the balance between exploration and exploitation. The searching individual $\overrightarrow{X}$'s position may be updated depending on the best location $\overrightarrow{X_b}$ in each iteration, and the fine-tuning parameters $\overrightarrow{W}$, $\overrightarrow{vb}$ and $\overrightarrow{vc}$ can change the individual's position. The inclusion of $rand$ in the formula permits individuals to generate search vectors at any direction. Therefore, Eq.(10) allows the searching individual to explore in all feasible directions towards the ideal solution, imitating slime mould's circular sector shape while approaching food.

## 2.1.2 Chaotic Slime Mould Algorithm

The proposed algorithm mentioned in this work follows slime mould algorithm's Eq.(1) to Eq.(9) initially, however, in equation Eq.(10), instead of utilizing $rand$ which is a random number, a chaotic local search approach based on search strategy is presented to increase the performance of SMA in achieving the optimal solution. The proposed approach speeds the search process and drives it to progress to a location where the optimal solution is more likely to be reached, boosting the ability of algorithm exploitation. Chaos is a prevalent event in natural nonlinear systems, and it's ergodic quality, notably traversing all states within a specified range without recurrence, is widely employed as a supplementary method to escape from local optimums. The sinusoidal chaotic map is employed in this study to produce appropriate chaotic sets. The map was generated as follows:

$$C_k = 2.3C_{k-1}sin(pi * C_{k-1}) \tag{11}$$

The chaotic map's initial value is set as 0.8 in this case and it's distribution along the iterations is illustrated in Figure 2.1.

## 2.2 Optimal Sizing and Placement of Multiple DG Units

### 2.2.1 Equilibrium optimizer

The EO is based on the property of mass-balance of a well mixed control volume which was first proposed in [91]. The general behaviour of mass-balance phenomenon can be expressed as a first order ordinary differential equation (ODE). Deducting the amount of mass leaving the system from the summation of quantity of mass entering the system and the amount being generated results in the change in mass over time, which can be equated as:

$$V\frac{dC}{dt} = QC_{eq} - QC + G \tag{12}$$

13

The symbol $C$ stands for the concentration in the control volume. $V \; dC/dt$ is the rate at which the mass in the control volume changes. The inward and outward flow rate is denoted by $Q$. When there is zero generation inside the experimental volume,that is referred to as concentration at equilibrium state and is denoted by $C_{eq}$.

Solving for $C$ results in:

$$C = C_{eq} + (C_0 - C_{eq})F + \frac{G}{\lambda V}(1 - \overrightarrow{F}) \tag{13}$$

Where

$$\overrightarrow{F} = e^{-\overrightarrow{\lambda}(t-t_0)} \tag{14}$$

The exponential term is an important factor affecting the main concentration updating. An optimum value of this term results in EO to have greater balance between exploration and exploitation. $t$ in Eq.(14) is directly related with the number of iterations and thus can be formulated as a function of iterations which decreases with iteration number.

$$t = (1 - \frac{Iter}{Max\_iter})^{a_2 \frac{Iter}{Max\_iter}} \tag{15}$$

The current and maximum number of iterations are represented as $Iter$ and $Max\_iter$, respectively. $a_2$ is a constant number that is utilized to control exploitation potential. By reducing the search speed, the convergence is guaranteed and at the same time it improves the exploration and exploitation capability of the technique.

Again,the term $t_o$ in Eq.(14) can be expressed as:

$$\overrightarrow{t}_0 = \frac{1}{\lambda}ln(-a_1 sign(\overrightarrow{r} - 0.5)[1 - e^{\overrightarrow{\lambda}t}]) + t \tag{16}$$

Exploration ability is directly governed by the constant $a_1$. Higher the value of $a_1$ means greater exploration capability but lower exploitation possibility and vise versa. Another factor affecting the exploration and exploitation is the $sign(\overrightarrow{r} - 0.5)$. The range of $r$ is between [0-1]. Replacing the expression of $t_o$ in Eq.(14) results in :

$$\overrightarrow{F} = a_1 sign(\overrightarrow{r} - 0.5)[e^{\overrightarrow{\lambda}t} - 1] \tag{17}$$

14

The initial concentration are assumed on the basis of the total number of particles and dimensions coupled with uniform random initialization in the following manner:

$$C_i^{initial} = C_{min} + rand_i(C_{max} - C_{min}) \quad i = 1, 2, ...n \tag{18}$$

The equilibrium state is reached when the algorithm converges, and it tends to the global optimum. Firstly, four possible candidates are assumed for providing a search pattern for the particles. Another particle is selected by taking the average of the four particles. The first four candidates mostly controls the global search while the fifth one assists the local search thus the equilibrium pool and candidates are formed.

$$\vec{C}_{eq,pool} = \{\vec{C}_{eq(1)}, \vec{C}_{eq(2)}, \vec{C}_{eq(3)}, \vec{C}_{eq(4)}, \vec{C}_{eq(ave)}\} \tag{19}$$

Furthermore, an optimum "generation rate" is proved to enhance the ability of EO for exploring, exploiting, and local minima avoiding which can be described as a first order exponential decay process as:

$$\vec{G} = \vec{G}_0 e^{-\vec{k}(t-t_0)} \tag{20}$$

$\vec{G}_0$ denotes the initial value, whereas $k$ denotes the decay constant. To achieve a more regulated and systematic search pattern and to limit the number of random variables, $k$ is taken as $\lambda$ and thus the equation becomes:

$$\vec{G} = \vec{G}_0 e^{-\vec{\lambda}(t-t_0)} = \vec{G}_0 \vec{F} \tag{21}$$

where

$$\vec{G}_0 = \overrightarrow{GCP}(\overrightarrow{C_{eq}} - \vec{\lambda}\vec{C}) \tag{22}$$

$$\overrightarrow{GCP} = \begin{cases} 0.5r_1 & r_2 \geq GP \\ 0 & r < p \end{cases} \tag{23}$$

Where $r_1$ and $r_2$ are taken arbitrarily in the range of [0-1] and the $\overrightarrow{GCP}$ vector is obtained by repeating the values obtained from Eq.(23). $\overrightarrow{GCP}$ (Generation rate Control Parameter) includes the potential of a generation term's contribution to the process of updating. Ultimately, The EO updating procedure will be as follows:

$$\vec{C} = \vec{C}_{eq} + (\vec{C} - \vec{C}_{eq}).\vec{F} + \frac{\vec{G}}{\vec{\lambda V}}(1 - \vec{F}) \tag{24}$$

The first term in Eq.(24) is an equilibrium concentration, where the second and third terms reflect the concentration fluctuations. The second term mainly explores the entire space globally for the best population whereas the third term seeks to improve the accuracy of the solutions.

## 2.2.2    Chaotic Equilibrium optimizer

The suggested approach in this work is based on the EO initially from Eq.(12) to Eq.(22). However, in Eq.(23), rather than employing $r_2$, which signifies a random value, a chaotic local search technique is introduced to improve the efficiency of EO in order to achieve the optimal solution. Chaos is a typical norm in dynamical nonlinear systems, and its stochastic property of spanning all phases within a given boundary without recurrence is widely used as an alternate technique for escaping from local optimums. The suggested technique accelerates the search strategy and directs it to a region where the best solution is prevalent. In this work, iterative chaotic map has been used to generate suitable chaotic sets. The map was developed in the following manner:

$$C_k = sin(pi * a)/C_{k-1} \tag{25}$$

In this context, the chaotic map's starting value and the value of $a$ are set to 0.7, and its distribution across iterations is seen in Figure 2.3. Hence, the Eq.(23) can be combined with chaos in the following manner:

$$\overrightarrow{GCP} = \begin{cases} 0.5r_1 & C_k \geq GP \\ 0 & r < p \end{cases} \tag{26}$$

The pseudo code of CEO is illustrated in Table 1.

## 2.3    Optimal Planning of Multiple Renewable Energy-Integrated Distribution System with Uncertainties

## 2.3.1    Artificial Hummingbird Algorithm

A hummingbird explores aspects such as the nectar amount and quality of certain flowers, as well as the nectar-refilling mechanism in order to pick a suitable source from a variety of food sources. Hummingbirds' unique flying skills and precise foraging methods for accessing food sources inspired

16

Table 1: Chaotic Equilibrium Optimizer pseudo code

| Algorithm : Pseudo-code of Equilibrium Optimizer |
|---|
| Define popsize and $Max\_Iter$ |
| Define higher bound and lower bound of the population |
| Initialize the population of particles |
| **while** $iter < maxiter$ |
| Assign $t$ using Eq.(15) and generate r and $\overrightarrow{\lambda}$ |
| **for** each candidate of $\overrightarrow{C}_{eq,pool}$ |
| Construct $\overrightarrow{F}$ using Eq.(14) |
| Construct $\overrightarrow{GCP}$ using Eq.(26) |
| Construct $\overrightarrow{G}_0$ using Eq.(22) |
| Construct $\overrightarrow{G}$ using Eq.(21) |
| Update $\overrightarrow{C}$ using Eq.(24) |
| **end** |
| Calculate each particles fitness value and update $\overrightarrow{C}_{eq,pool}$ |
| Return the best $\overrightarrow{C}_{eq(1)}$ |
| $Iter= Iter+1$ |
| **end** |
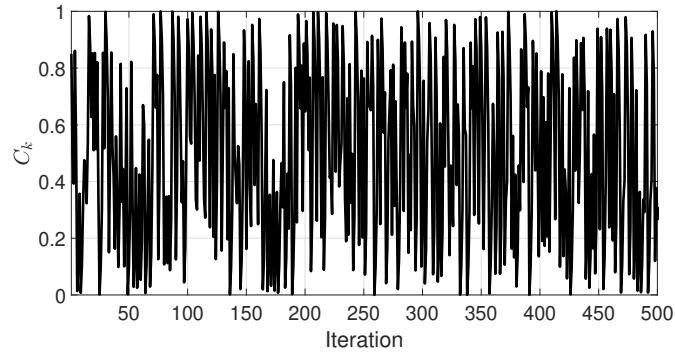


Figure 2.3: Iterative chaos map

this algorithm, which varies from prior algorithms in terms of search domain diversity. The different flying patterns ensure that the algorithm has a high exploitation probability and exploration ability. Besides, a unique component called the visit table is also included in order to simulate the hummingbird's memory for identifying suitable food sources. Hummingbirds employ three foraging approaches and three flying skills to collect food from sources [92]. The three different flying patterns are known as axial, diagonal, and omnidirectional, as well as the three different search strategies are known as guided foraging, territorial foraging, and migration foraging. The following section includes three mathematical models that simulate three hummingbird foraging habits.

Initialization

A swarm of $n$ hummingbirds is arbitrarily assigned to $n$ food sources, as follows:

$$x_w = LB + rand(UB - LB) \qquad w = 1..., n \tag{27}$$

where $LB$ and $UB$, respectively represent the upper and lower bounds of a $d$-dimensional problem. $rand$ is a random vector in the range [0, 1] and the location of the $w^{th}$ food supply that provides the solution to the particular objective is represented by $x_w$. The visit table of the source of food can be specified as :

$$VT_{w,e} = \begin{cases} 0, & \text{if } w \neq e \quad w = 1..., n \\ null, & \text{if } w = e \quad e = 1..., n \end{cases} \tag{28}$$

when $w = e$, the value of $VT_{w,e}$ becomes null which means that a hummingbird is collecting its food from its particular source. Moreover, when $w \neq e$ the value of $VT_{w,e}$ becomes zero which implies that the $e^{th}$ food source has been very recently searched by the $w^{th}$ hummingbird in the current iteration.

Guided Foraging

Every hummingbird has a general tendency for foraging the source of food with the most nectar volume, which implies that an intended source must possess a high replenishing rate of nectar and a lengthy interval without any visit. Three flying methods: omnidirectional, diagonal, and axial flights are utilized by providing a direction switch vector during foraging. This vector is utilized to determine if one or more $d$-dimension space directions are accessible. Most birds can fly omnidirectionally, but hummingbirds can also glide axially and diagonally. The axial flight can be expressed as:

$$D^{(w)} = \begin{cases} 1, & \text{if } w = randi([1, d]) \quad w = 1, ..., d \\ 0, & \text{else} \end{cases} \tag{29}$$

The diagonal flight can be expressed as:

$$D^{(w)} = \begin{cases} 1, & \text{if } w = Pp(j), j \in [1, k] \\ & Pp = randperm(Kp) \\ & Kp \in [2, [r_1 \cdot (d-2)] + 1] \\ 0, & \text{else } w = 1, ..., d \end{cases} \tag{30}$$

The omnidirectional flight can be expressed as :

Table 2: Artificial hummingbird algorithm pseudo code

| Algorithm : Pseudo-code of AHA |
|---|
| Define $N_{pop} = n$ = Population size |
| Define $N_{iter,max}$ |
| Define higher and lower bound of the population |
| Initialize the population using Eq.(27) |
| **while** $tp \leq N_{iter,max}$ |
|     **for** Each population calculate direction switch vector $D$ |
|     **if** rand $\leq 1/3$ |
|     Follow diagonal flight using Eq.(30) |
|     **else if** rand$\leq 2/3$ |
|      Follow omnidirectional flight using Eq.(31) |
|     **else** Follow axial flight using Eq.(29) |
|     **end if** |
|     **end for** |
|         **for** Each population update foraging behaviour |
|         **if** rand $\leq 0.5$ |
|         Follow guided foraging using Eq.(29) to Eq.(34) |
|         **else if** Follow territorial foraging using Eq.(35), Eq.(36) |
|         **end if** |
|         **if** $tp = 2n$ |
|         Follow migration foraging using Eq.(37) |
|         **end if** |
|         **end for** |
| Update positions |
| Return the best fitness value |
| $tp = tp+1$ |
| **end while** |

$$D^w = 1 \qquad i = 1, ...., d \tag{31}$$

where, an arbitrary integer between 1 and $d$ is returned by $randi$. An arbitrary permutation sequence of integers between 1 and $Kp$ is generated by $randperm(Kp)$. $r_1$ is a random value between 0 and 1. Therefore, a food source is upgraded in terms of the target food source, which is identified from the current sources. Hence, the equation to replicate directed foraging is as follows:

$$vp_w = x_{w,tar}(tp) + a.D.(x_w(tp) - x_{w,tar}(tp)) \tag{32}$$

$$a \sim N(0,1) \tag{33}$$

$x_w(tp)$ defines the location of the $w^{th}$ source of food at current iteration $tp$, $x_{w,tar}(tp)$ is the location of the source of food that the $w^{th}$ hummingbird plans to consume from, and that denotes a normal distribution with a mean value of zero and a standard deviation of one. Moreover, Eq.(32) allows each present source to modify its location with relation to the intended source of food and

replicates guided foraging in hummingbirds using various flying patterns. Hence, the location of the $w^{th}$ food source is updated as follows:

$$x_w(tp+1) = \begin{cases} x_w(tp) & \text{if } f(x_w(tp)) \leq f(vp_w(tp+1)) \\ v_w(tp+1), & \text{if } f(x_w(tp)) > f(vp_w(tp+1)) \end{cases} \tag{34}$$

where $f$ signifies the fitness value of the function. According to Eq.(34), if the candidate food source's nectar-refilling rate is greater than the present one, the hummingbird leaves the present source of food and consumes from the candidate food source following Eq.(32). The visit table is a key component of the AHA algorithm that retains the information about the visit to the sources of food. The visit table records how long each food source has been undiscovered, and a long undiscovered period indicates a high degree of visit. Through Eq.(32), every bird of the swarm accesses its desired source of food. When a bird undergoes guided foraging utilizing Eq.(32), keeping in mind of its targeted source of food during each iteration, the visit levels of all the other sources are increased by one.

Territorial Foraging

When the nectar of the flower has been exhausted, a hummingbird prefers to seek out a new source of food than it is to visit other current food sources. As a result, a hummingbird might easily migrate to an adjacent location within its own region, where a new food supply may be discovered. The mathematical equation for modelling hummingbirds' territorial foraging behaviour is as follows:

$$vp_w(tp+1) = x_w(tp) + bp.D.x_w(tp) \tag{35}$$

$$bp \sim N(0, 1) \tag{36}$$

The territorial factor, $bp$, has a mean value of zero and a standard deviation of one and follows a normal distribution. By using its specific flight talents as Eq. 35, every hummingbird can swiftly identify a new source of food in its nearby surroundings.

Migration Foraging

If the number of iterations surpasses the previously specified migration coefficient value, the bird which is at the source of food with the lowest replenishing rate of nectar will arbitrarily look for a new source of food within the territory. A hummingbird's migratory foraging to a destination might be described as follows:

$$x_{wor}(tp+1) = LB + rand(UB - LB) \tag{37}$$

Here, $x_{wor}$ is the source of food with the lowest replenishing rate of nectar. The following is a preferred definition for the migration coefficient in terms of population size ($n$):

$$tp = 2n \tag{38}$$

According to Eq. (32), in the initial stages of iterations, exploration is stressed due to the significant distance between food sources, but as the number of iterations increases, the distance iteratively reduces, and therefore exploitation is prioritized.

# Chapter 3

## 3 Modelling and Problem Formulation

### 3.1 VSM

Voltage stability margin ($VSM$) [93] correlates voltage collapse and branch loading of a distribution network. Fig. 3.4 represents a radial feeder with a number of $k$ branches whose loading indices, $L_k$ can be formulated as:

$$L_k = (2\frac{V_v}{V_q}cos\delta_{qv} - 1)^2 \tag{39}$$
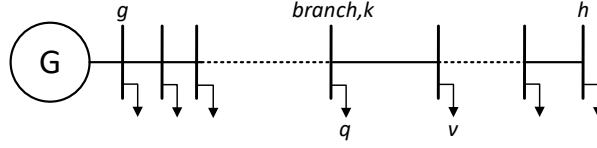


Figure 3.4: Radial feeder

The voltage magnitudes of bus $q$ and bus $v$ are represented by $V_q$ and $V_v$, respectively, whereas $\delta_{qv}$ specifies the phase angle difference between these buses. Now, $VSM$ can be calculated as the product of all loading indices for all branches of the given radial feeder.

$$VSM = \prod_{l=\Omega} L_k \tag{40}$$

where $\Omega$ covers up all the branches of the radial feeder from the starting bus $g$ to the ending bus $h$. If there are several feeders in a system, then $VSM_{sys}$ is calculated as the $VSM$ of the feeder with the minimum value.

$$VSM_{sys} = min(VSM_1, VSM_2, VSM_3, ...; VSM_{ssf}) \tag{41}$$

where $ssf$ represents the system's total number of feeders.

### 3.2 Operational Constraints

Some operational constraints should be maintained during the whole optimization. To represent these constraints, following conditions are adopted for our works which are presented next.

i. **Power flow balance** : Total real power generation ($P_{gen}$) and reactive power generation ($Q_{gen}$) should be equal to the sum of real power loss ($P_{loss}$) and reactive power loss ($Q_{loss}$) and

real and reactive load demand $(P_{load}, Q_{load})$, respectively.

$$\sum_{n=1}^{N_G} P_{gen} = \sum_{i=1}^{N_L} P_{load} + \sum_{l=1}^{N_{Line}} P_{loss} \tag{42}$$

$$\sum_{n=1}^{N_G} Q_{gen} = \sum_{i=1}^{N_L} Q_{load} + \sum_{l=1}^{N_{Line}} Q_{loss} \tag{43}$$

where $N_G$ represents number of generators and $N_L$ denotes total number of load buses, and $N_{Line}$ represents the total number of branches of the network,

ii. **Voltage limit** : Voltage $(V_i)$ at each bus should be kept within a permitted range, as illustrated in in Eq.(44). Generally, within 10% from the nominal voltage value is allowed.

$$V_{i-min} \leq V_i \leq V_{i-max} \tag{44}$$

iii. **Voltage stability margin(VSM) limit** : The $VSM_{sys}$ value of a system should lie between 0.67 to 1.

$$0.67 \leq VSM_{sys} \leq 1 \tag{45}$$

iv.**Power flow limit** : The transmitted apparent power through branch, $l$ of distribution system must not exceed maximum thermal limit.

$$S_l \leq S_{l-max} \tag{46}$$

v. **Load priority limit** : Load priority limit, $P_{load-limit}$ represents the minimum amount of load that must be kept in an islanded distribution system after load-shedding. This can be described as follows:

$$P_{load-limit_{(i)}} = P_i * (\%)Loadlevel * P_{Lim(i)} \tag{47}$$

where, $P_{Lim(i)}$ denotes the minimum percentage of load that must be maintained in each of the buses throughout 24 hours. These values were chosen at random prior to the optimization. Therefore, the remaining load $P_{rem-i}$ at each bus can't be less than $P_{load-limit(i)}$, as stated below:

$$P_{load-limit(i)} \leq P_{rem(i)} \leq P_i \tag{48}$$

vi. **DG penetration limit** : Each DG must have a minimum and maximum active and reactive output power limit value, as stated value:

$$P_{DGi}^{min} \leq P_{DGi} \leq P_{DGi}^{max} \tag{49}$$

$$Q_{DGi}^{min} \leq Q_{DGi} \leq Q_{DGi}^{max} \tag{50}$$

However, for the purpose of this study, the minimum and maximum rating of each DG has been considered as 0.1 MVA to 1.48 MVA with a constant power factor of 0.9 per unit (p.u).

vii. **RDG Capacity Constraints** The active power capacity of each RDG farm is limited to a specific maximum.

$$N_{RDGi} * P_{RDGi} \leq NRDGi_{max} * P_{RDGi} \tag{51}$$

where $N_{RDGi}$ is the number of elementary RDG units which comprises the RDG farm at location $i$; $P_{RDGi}$ is the rated power of elementary RDG unit at location $i$; and $NRDGi_{max}$ is the maximum number of elementary RDG units at location $i$.

## 3.3 Optimal Load-Shedding in Distribution System

### 3.3.1 Fitness Function

The fitness function of this study aims to evaluate the optimal load shedding technique in islanded systems by maintaining the maximum allowable loads along with system's acceptable voltage profile. Hence, the fitness function is written as:

$$fitness = max(\frac{P_{rem}}{P_{gen}} + VSM_{sys}) \tag{52}$$

$$P_{rem} = \sum_{i=1}^{i} P_{rem(i)} \tag{53}$$

where, $i$ denotes individual bus numbers and $P_{gen}$ denotes total real power generation of a particular island. Remaining load, $P_{rem}$ of a particular bus is the amount of load that will be present at that bus after load shedding.

The solution set considered for the purpose of optimization is the remaining load $(P_{rem(i)})$ array which includes the amount of load maintained for each bus and has the same size as the number of buses in the islanded system under investigation. The $\frac{P_{rem}}{P_{gen}}$ term in fitness function has been used to assure that the quantity of remaining load is maximized with respect to total power generation, leading in the least amount of total shedded load while satisfying all the operational constraints.

24

$VSM_{sys}$, which is a voltage stability indicator, can identify the critical load in an islanded network by utilizing the voltage profile of the buses. The initial population set is generated as follows:

$$P_{rem(i)} = rand(P_i - P_{load-limit(i)}) + P_{load-limit(i)} \qquad (54)$$

where $P_i$ denotes the base load at $i^{\text{th}}$ bus before load shedding and $P_{load-limit(i)}$ denotes the minimum amount of load that must be maintained in $i^{\text{th}}$ bus during load shedding.

Hence, the position update Eq.(10) is modified with chaotic sinusoidal map as follows:

$$\overrightarrow{X(t+1)} = \begin{cases} rand(P_i - P_{load-limit(i)}) + P_{load-limit(i)}, & rand < z \\ \overrightarrow{X}_b(t) + \overrightarrow{vb}.(\overrightarrow{W}.\overrightarrow{X_A(t)} - \overrightarrow{X_B(t)}), & C_{(k+1)} < p \\ \overrightarrow{vc}.\overrightarrow{X(t)}, & C_{(k+1)} \geq p \end{cases} \qquad (55)$$

Where $P_i$ is considered as the higher bound of the population while $P_{load-limit(i)})$ is considered as the lower bound. For the purpose of this work, BSA, original SMA and the proposed CSMA technique is conducted to demonstrate performance enhancements of CSMA.

## 3.3.2 Islanding scenarios of IEEE 33 and 69 bus distribution system

This article analyzes the IEEE 33 bus and the IEEE 69 bus radial distribution system for three islanding cases. Figure 3.5 and Figure 3.6 depict the islanding scenarios and DG placements for Island-1 and Island-2, which were developed for IEEE 33 bus system. For Island- 1 and Island-2, four DG units are taken into account, two of which are constant generators (DG2 and DG4) while the other two are photovoltaic (PV) generators. With a total load demand of 3.715 MW and 2.3 MVar for the IEEE 33 bus radial distribution system in non islanded scenario, the maximum supply capacity of all four DG units is 1.83 MW.

Furthermore, Island-3 was developed for IEEE 69 bus distribution system. The baseload power demand for IEEE 69 bus is 3.8019 MW and 2.6946 MVar without islanding . Three DG units are designated as constant generators (CG) for Island-3 as shown in Figure 3.6, with a total generation of 1.747 MW when all DG units are operational. Table 3 and Table 4 displays the rated maximum power of all the DGs under consideration. As shown in Figure 3.8, the individual load profiles along a typical day of all the islands are assumed to be the same. The PV generator's daily power generation over the course of 24 hours is depicted in Figure 3.9. It is also assumed that all PV's power generating characteristics over 24 hours are of the same type with varied ratings.
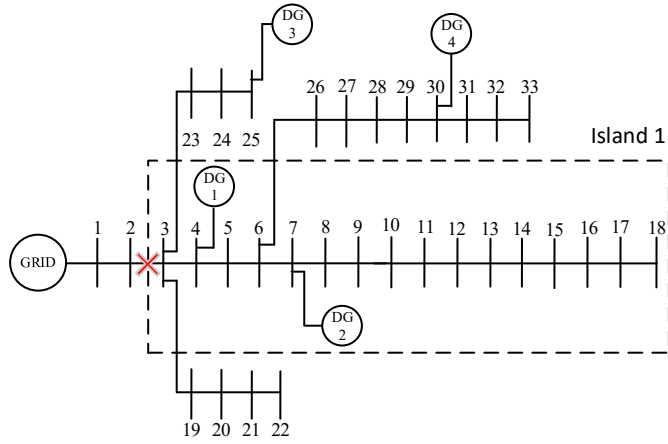
Figure 3.5: One-line Diagram of Island-1 for IEEE 33 bus system
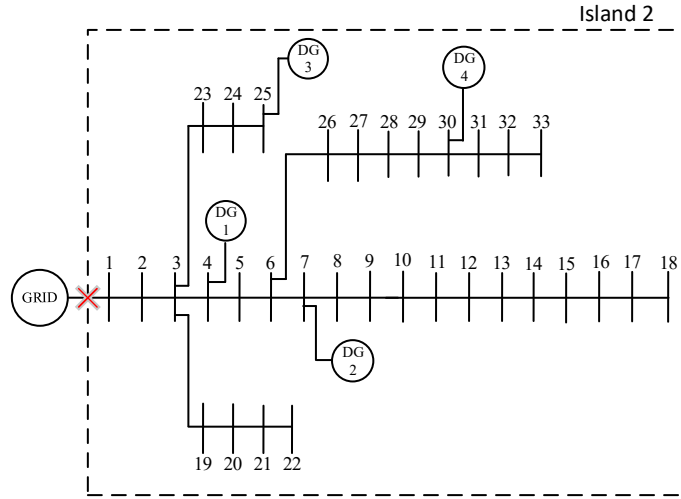


Figure 3.6: One-line Diagram of Island-2 for IEEE 33 bus system

## 3.4  Optimal Sizing and Placement of Multiple DG Units

### 3.4.1  Fitness Function

**Optimal DG sizing and placement**

The objective of the fitness function adopted in this work is to identify the optimal positioning and sizing of DGs in order to minimize total active power loss and total voltage deviation while satisfying all the operational constraints mentioned above.

$$fitness = minimize(\frac{P_{Loss}}{P_{base-Loss}} + V_{deviation}) \tag{56}$$

$$P_{Loss} = \sum_{l=1}^{l} |I_l|^2 R_l \tag{57}$$

26
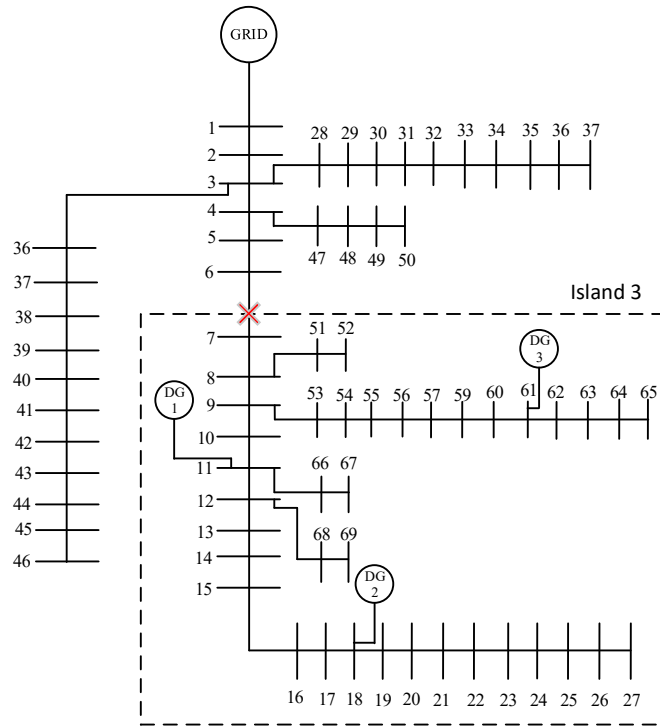
Figure 3.7: One-line Diagram of Island-3 for IEEE 69 bus system
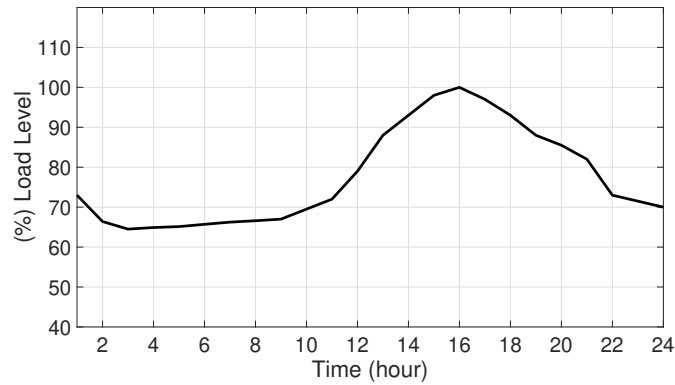


Figure 3.8: Daily load profile
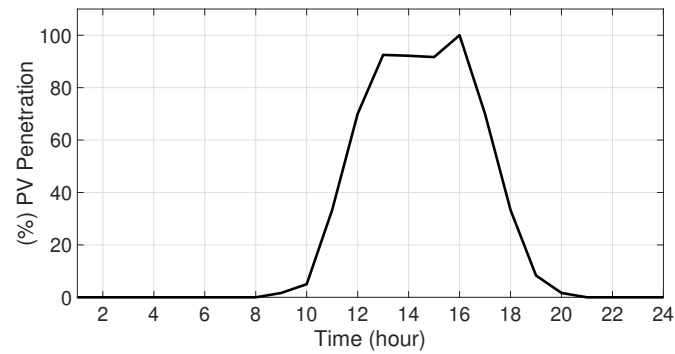


Figure 3.9: Daily PV generation

$$V_{deviation} = \sum_{i=1}^{i} |V_i - V_M| \tag{58}$$

27

Table 3: IEEE 33 Bus system DG specifications

|  | Island 1 and island 2 | | |
|---|---|---|---|
| Name | Type | Location | Active power rating (MW) |
| DG1 | PV | 4 | .03 |
| DG2 | CG | 7 | .8 |
| DG3 | PV | 25 | .6 |
| DG4 | CG | 30 | .4 |

Table 4: IEEE 69 Bus system DG Specifications

|  | Island 3 | | |
|---|---|---|---|
| Name | Type | Location | Active power rating (MW) |
| DG1 | CG | 11 | .259 |
| DG2 | CG | 18 | .551 |
| DG3 | CG | 61 | .937 |

Where, $P_{base-Loss}$ represents the amount of loss in the absence of DGs, $P_{Loss}$ signifies the amount of loss after penetrating DGs, $V_M$ equals 1.0 p.u and $V_i$ represents the voltage magnitude (p.u) at $i^{\text{th}}$ bus, and $I_l$ and $R_l$ denotes the current flow and the resistance of the $l^{\text{th}}$ branch.

**Load shedding optimization**

The fitness function used for optimal load shedding strategy determines the ideal shedded load while preserving the maximum amount of loads and the appropriate voltage profile of the islanded network. Therefore, the fitness function is expressed as follows:

$$fitness = maximize(\frac{S_{rem}}{S_{gen}} + VSM_{sys}) \tag{59}$$

$$S_{rem} = \sum_{i=1}^{i} S_{rem(i)} = \sum_{i=1}^{i} S_i - S_{s(i)} \tag{60}$$

$$P_{rem(i)} = pf(i) * S_{rem(i)} \tag{61}$$

$$Q_{rem(i)} = \sqrt{(S_{rem(i)})^2 - (P_{rem(i)})^2} \tag{62}$$

where $i$ indicates individual bus numbers, $pf(i)$ denotes the power factor at $i^{\text{th}}$ bus, $S_{gen}$ signifies total apparent power generation of an island, $S_{rem(i)}$ signifies the remaining apparent load at $i^{\text{th}}$ bus, $P_{rem(i)}$ represents the remaining real load at $i^{\text{th}}$ bus and $Q_{rem(i)}$ denotes the remaining reactive load at $i^{\text{th}}$ bus.

The optimal solution set evaluated is the shedded load $(S_{s(i)})$ array, which contains each node's amount of load to be shed. Furthermore, $S_i$ denotes the total apparent load demand at $i^{\text{th}}$ bus before load shedding. The maximum quantity of remaining apparent load, $S_{rem}$ has been

employed to ensure that the remaining load quantity is maximized, culminating in the minimal amount of total load to be shed, $S_s$ while agreeing all the operational constraints. Notably, the $(1 - S_{load-limit(i)})$ term is regarded as the solution set's upper bound. Moreover, $VSM_{sys}$ can detect the susceptible branch of an islanded network by analyzing the voltage magnitudes of each of the buses. Section 3.1 covers through the detailed expression for $VSM_{sys}$. The initial population was initiated as follows:

$$S_{S(i)} = rand(1 - S_{load-limit(i)}) \tag{63}$$

## 3.5 Optimal Planning of Multiple Renewable Energy-Integrated Distribution System with Uncertainties

### 3.5.1 Modelling

Renewable power is primarily affected by weather conditions such as solar irradiation, temperature, wind speed, etc. As a result, before planning the integration of RDG units into electrical networks, the uncertainties and unpredictable behaviour of renewable output power should be assessed extensively. Monte carlo simulation method is a probabilistic approach is the most used method to characterize power system uncertainties. Besides, weibull and beta functions were used to model the uncertainty of wind speed and solar irradiance, respectively. For the purpose of this study, historical weather information for one year has been collected to obtain a typical annual profile for stochastic behaviour pattern of solar irradiance and wind speed [94].

**Modelling of WT**

A wind turbine's power generated, $P_{WT}$, can be formulated as :

$$P_{WT}\ (v) = \begin{cases} 0 & for\ v \leq v_{ci} \\ \frac{v-v_{ci}}{v_n-v_{ci}} * P_{WTR} & for\ v_{ci} < v \leq v_n \\ P_{WTR} & for\ v_n < v \leq v_{co} \\ 0 & for\ v \geq v_{co} \end{cases} \tag{64}$$

The stochastic nature of wind resources in a specific location can be evaluated by utilizing the following weibull probability density function:

$$f_v(v) = K/C * (v/C)^{K-1} * e^{-(v/C)^K} \tag{65}$$

The weibull function's cumulative distribution function can be expressed as Eq.(66) while wind
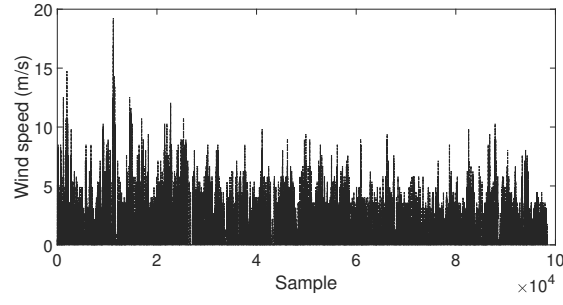
Figure 3.10: Wind speed test data [94]

speed can be determined from its inverse as shown in Eq.(67).

$$F_v(v) = 1 - e^{-(v/C)^K} \tag{66}$$

$$v = C * [-ln(r)]^{(1/K)} \tag{67}$$

where, $k$ and $C$ are the shape factors whose expected values can be found using the average and standard deviation (std) of the wind speed measurements in a period $t$ can be expressed as Eq.(68) and Eq.(69).

$$K^t = (\sigma_v^t/\mu_v^t)^{-1.086} \tag{68}$$

$$C^t = \mu_v^t/\Gamma(1 + 1/K^t) \tag{69}$$

Weibull PDF can be expressed in discrete form by sub-dividing the considered time interval $t$ into $N_v$ states. By considering $g$ as the inverse of $N_v$, Eq.(65) and Eq.(68) can be re-written and the forecasted WT power can be formulated as Eq.(70).

$$P_{WT} = [\sum_{g=1}^{N_v} P_{WTg} * f_v(v_g^t)]/[\sum_{g=1}^{N_v} f_v(v_g^t)] \tag{70}$$

where, $v = v_g^t$ and $f_v(v_g^t)$ refers to the probability of wind speed at $t^{th}$ time interval for the $g^{th}$ state.

**Modelling of PV**

Power generated from PV units significantly depends on solar irradiance and it can be formulated
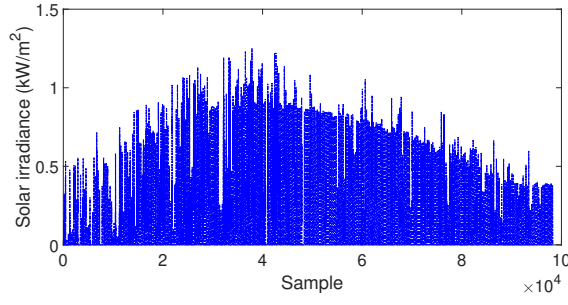
Figure 3.11: Solar irradiance test data [94]

as:

$$P_{PV}\ (G) = \begin{cases} (P_{PVR} * G^2)/(G_{STC} * R) & for\ G < R_c \\ (P_{PVR} * G)/G_{STC} & for\ G > R_c \end{cases} \tag{71}$$

The beta probability density function is used to achieve realistic PV unit modelling by considering the stochastic behaviour of solar irradiation.

$$f_s\ (G) = \begin{cases} [\Gamma(\alpha + \beta)/(\Gamma(\alpha) * \Gamma(\beta))] * G^{(\alpha+1)} * (1-G)^{(\beta-1)} \\ \qquad for\ 0 \le G \le 1, \alpha \ge 0, \beta \ge 0 \\ 0 \qquad otherwise \end{cases} \tag{72}$$

where $\alpha$ and $\beta$ are the shape factors of beta function which can be determined by considering the average and standard deviation of the solar irradiance as shown in Eq.(73) and Eq.(74).

$$\beta^t = (1 - \mu_G^t) * [(\mu_G^t * (1 + \mu_G^t)/(\sigma_G^t)^2) - 1] \tag{73}$$

$$\alpha^t = (\mu_G^t * \beta^t)/(1 - \mu_G^t) \tag{74}$$

Beta PDF can be taken into discrete form by sub-dividing the considered time interval $t$ into $N_s$ states. Thus, re-writing the Eq.(72) while considering $g$ from 1 to $N_s$, the forecasted PV generated power can be formulated as Eq.(75).

$$P_{PV} = [\sum_{g=1}^{N_s} P_{PVg} * f_s(S_g^t)]/[\sum_{g=1}^{N_s} f_s(S_g^t)] \tag{75}$$

where, $f_s(G_g^t)$ refers the solar irradiance probability at $t^{th}$ time interval for $g^{th}$ state.

**Load Modelling**

The normal probability distribution function can be used to define load patterns for each hour of a specified daily load.

31
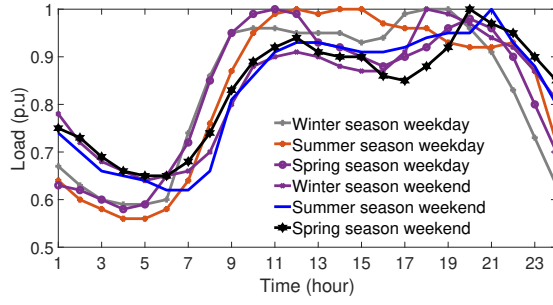
Figure 3.12: IEEE reliability test system (RTS) load data [95]

$$f_L(L) = \frac{1}{\sqrt{2\pi}\sigma_L} e^{-\frac{(L-\mu_L)^2}{2\sigma_L^2}} \tag{76}$$

$$f_L(L) = (1/2)\left(1 + erf((L - \mu_L)/\sqrt{2}\sigma_L\right) \tag{77}$$

$$L = \mu_L + \sqrt{2}\sigma_L * erf^{-1}(2r - 1) \tag{78}$$

where $L$ is a random variable that represents load, and $\mu_L$, $\sigma_L$ represent the average and std of $L$, correspondingly. $erf(.)$ and $erf^{-1}(.)$ signify the error and inverse error functions, respectively, and $r$ is a random number between 0 and 1.

Hour, $t$ is divided into $N_L$ states for convenience, and the associated load and probability value for each state can be determined using Eqs.(77) and (78), accordingly. $L$ can be reformulated as :

$$L^t = \sum_{g=1}^{N_L} L_g f_L(L_g^t) / \sum_{g=1}^{N_L} f_L(L_g^t) \tag{79}$$

where $L_g^t$ refers the load of state $g$ at hour $t$; $L_g$ is the load level at state $g$ and $f_L(L_g^t)$ is the probability of the load level of the state $g$ at hour $t$. The load data for different seasons are collected from [95].

## 3.5.2   Fitness Function

The fundamental objective of this work is to maximize the techno-economic benefits of RDGs in distribution networks. Several aspects are explored to comprehend the simulation, including active power loss minimization, bus voltage improvement, network voltage stability margin (VSM) enhancement, and yearly economic loss reduction. Using the weighted sum approach, these four evaluation criteria can be integrated into a single objective function.

$$OF = min\ (\omega_1 * OF_1 + \omega_2 * OF_2+ \tag{80}$$
$$\omega_3 * OF_3 + \omega_4 * OF_4)$$

where, $OF_1$, $OF_2$, $OF_3$, $OF_4$ denotes the reduction in total active power losses, strengthening bus voltages by minimizing voltage deviation, improvement of VSM of the network, increasing the amount of total annual energy saving, respectively. $\omega_1$, $\omega_2$, $\omega_3$, $\omega_4$ represents the weighted factors assigned to $OF_1$, $OF_2$, $OF_3$, $OF_4$ respectively and total sum of absolute values of $\omega_1$, $\omega_2$, $\omega_3$, $\omega_4$ is considered to be equal to 1. It should be noted that all weighted factors are considered to be the same with a value of 0.25. Furthermore, all the values of Eq.(80) are in per unit (p.u.) values. The four components of $OF$ can be expressed mathematically like following equations.

$$OF_1 = P_{loss} = \sum_{b=1}^{N_{BR}} P_{loss,b} \tag{81}$$

$$OF_2 = V_D = \sum_{i=1}^{N_B} |V_i - V_i^{ref}| \tag{82}$$

$V_D$ is considered as the total voltage deviation while $V_i$ denotes the actual voltage magnitude (p.u) at $i^{\text{th}}$ bus and $V_i^{ref}$ represents 1.0 (p.u) of voltage magnitude.

$$OF_3 = \frac{1}{VSM_{sys}} \tag{83}$$

$$OF_4 = \frac{1}{TAES} \tag{84}$$

where,

$$TAES = AEL_{T,no\ DG} - AEL_{T,DG} \tag{85}$$

$$AEL_{T,noDG} = P_{loss,no-DG} * C_E * 8760 \tag{86}$$

$$AEL_{T,DG} = P_{loss,RDG} * C_E * 8760$$
$$+[(C_{DG} * \sum_{m=1}^{N_{DG}} P_{DG,m})/CRF] \tag{87}$$

$$CRF = [R * (1 + R)^{T_{DG}}]/[(1 + R)^{T_{DG}} - 1] \tag{88}$$

### 3.5.3 Control Variables

Positions, or indices of connected buses, and the number of elementary RDG units that should be connected at these buses are the control variables in this optimization problem. Considering these two variables, the RDG farms' optimum rated power can be determined as:

$$P_{RDGF} = N_{RDG} * P_{RDG} \tag{89}$$

where $P_{RDGF}$ is the RDG farms' total rated power, $N_{RDG}$ is the number of elementary RDG units that make up an RDG farm (WT farm or PV farm), and $P_{RDG}$ is the rated power of an elementary RDG unit.

## 3.6 Test Systems Description

IEEE 33 bus and IEEE 69 bus distribution systems are employed as test systems in this work.
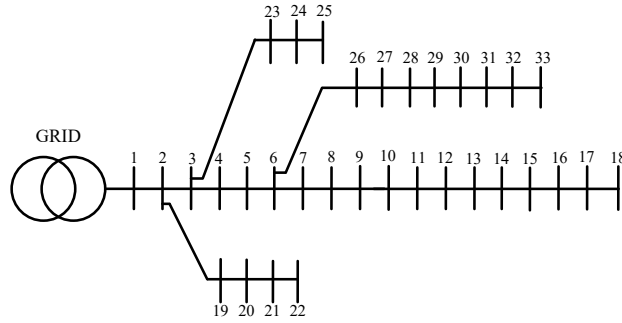


Figure 3.13: IEEE 33 bus distribution system

The one-line schematics for the IEEE 33 and IEEE 69 buses are shown in Fig. 3.13 and Fig. 3.14, respectively. The total load demand of the IEEE 33 bus system is 3.715 MW and 2.3 MVAr, whereas the total load demand of the IEEE 69 bus system is 3.802 MW and 2.695 MVAr. Furthermore, under normal operating conditions, total active power loss is 202.5 kW for the 33 bus system and 220.3 kW for the 69 bus system.
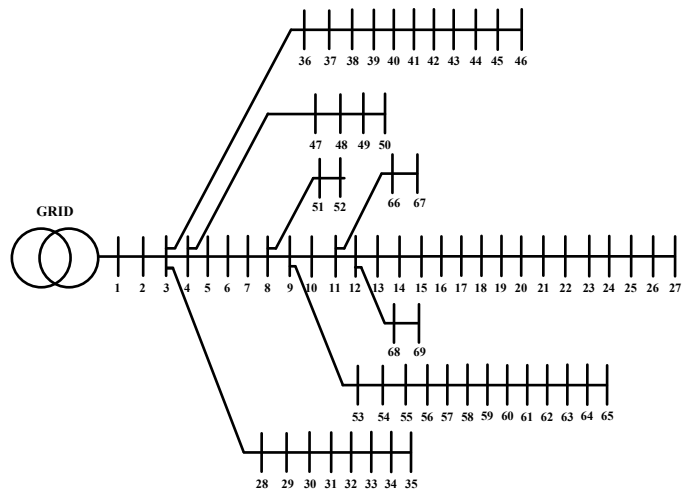
Figure 3.14: IEEE 69 bus distribution system

# Chapter 4

## 4 Results Analysis

### 4.1 Optimal Load-Shedding in Distribution System

The proposed optimal load shedding technique employing the Chaotic slime mould algorithm (CSMA) is simulated and evaluated against original SMA and BSA employing identical methodologies. The purpose of this research is to develop a chaotic optimization method for optimal load shedding and compare it to SMA and BSA in order to demonstrate the superiority of the proposed approach. To ensure a fair comparison, the total number of iterations (1000) and initial population size (50) are maintained constant across all three methods for each island. Moreover, the stopping criterion for the algorithms is set to be the maximum number of iterations. A comparative study of CSMA, SMA, and BSA in terms of elapsed time and best fitness values obtained while maximizing the objective function is presented in the following section. Additionally, for nonparametric statistical analysis purposes, each algorithm is evaluated 30 times for Island-1, with the average, best and the worst results being reported.

### 4.1.1 Comparative results of the algorithms

Table 5 shows each algorithm's fitness value, remaining load, VSM, and computational time required for each of the islands considered. It appears that, for all the islanding scenarios, slime mould based optimization technique performs superior to BSA. More notably, the suggested chaotic slime mould method surpasses the fitness values achieved in SMA in each islanding instance, indicating that using chaos instead of random numbers leads to a superior fitness value with less computing time for load shedding optimization. Furthermore, the findings in Table 5 show that CSMA assures greater remaining load in the system with higher voltage stability margin values than SMA and BSA. In Island-1, CSMA outperforms BSA and SMA by a small margin, whereas on Island-2 and Island-3, CSMA performs significantly better. Hence, it has been discovered that as the number of buses on an island increases, the fitness value difference between the algorithms grows and CSMA performs far effectively. In addition, it was revealed that the time disparities among the algorithms are insignificant for Island-1, which has the smallest network among all the islands. Furthermore, in terms of elapsed time, BSA outperforms SMA, while CSMA remains the best of the three optimization approaches in Island-1. Likewise, CSMA's fitness value outclasses BSA and SMA on the other two islands, with 33 and 40 buses on Island-2 and Island-3, respectively. The

computational time disparities between the algorithms rose considerably and CSMA outperformed both BSA and SMA.

Table 5: Fitness values and corresponding elapsed time

| Algorithm | Parameter | Island-1 | Island-2 | Island-3 |
|---|---|---|---|---|
| BSA | Fitness Value | 1.9164 | 1.9232 | 1.9782 |
| | Remaining load (MW) | 0.8229 | 1.8179 | 1.7157 |
| | VSM | 0.9250 | 0.9299 | 0.9994 |
| | Elapsed time (s) | 49.70 | 84.93 | 103.77 |
| SMA | Fitness Value | 1.9234 | 1.9250 | 1.9872 |
| | Remaining load (MW) | 0.8239 | 1.818 | 1.728 |
| | VSM | 0.9308 | 0.9316 | 0.9981 |
| | Elapsed time(s) | 53.23 | 74.84 | 89.57 |
| CSMA | Fitness Value | **1.9265** | **1.9320** | **1.9915** |
| | Remaining load (MW) | 0.8243 | 1.8201 | 1.7347 |
| | VSM | 0.9334 | 0.9373 | 0.9986 |
| | Elapsed time (s) | 49.94 | 70.30 | 83.31 |

To adequately compare the algorithms, 30 independent runs of each algorithm were performed on Island-1 with the same number of iterations and the same initial population. Table 6 shows the average, best, and worst values of each scheme in terms of fitness value and computing time. The recommended CSMA had a better average and best fitness value throughout the independent runs compared to BSA and SMA. Moreover, it is found that, the worst CSMA fitness (1.9200) is much better than the best BSA fitness (1.9164) and it also equals the average SMA fitness (1.9200). In terms of elapsed time, BSA outclasses SMA only in Island-1 while CSMA remains the best amongst the three in every test system. Moreover, Table 5 depicts that as the network becomes more intricate and larger, time consumption becomes an even more important factor in favoring CSMA over the other two algorithms.

Table 6: Comparative results of 30 runs in Island-1

| Parameter | Algorithm | Elapsed Time(s) | Fitness Value |
|---|---|---|---|
| Best result | BSA | 49.70 | 1.9164 |
| | SMA | 50.50 | 1.9234 |
| | CSMA | 48.28 | **1.9265** |
| Average result | BSA | 52.46 | 1.9115 |
| | SMA | 52.96 | 1.9200 |
| | CSMA | 50.57 | **1.9220** |
| Worst result | BSA | 57.56 | 1.9039 |
| | SMA | 56.39 | 1.9164 |
| | CSMA | 55.64 | **1.9200** |

## 4.1.2 Nonparametric Statistical Analysis

For further investigation, the three algorithms are subjected to non-parametric statistical analysis among the 30 independent runs each for Island-1.

The one-sample Kolmogorov–Smirnov (KS) test is utilized where the null hypothesis, H0 implies that the samples have a normal distribution. The opposing hypothesis, H1, implies that the samples

do not conform to a normal distribution at a significance level of 0.05. The results of the one-sample KS test are shown in Table 7. CSMA-based algorithm outperforms the BSA and SMA in terms of mean value. Evidently, the standard deviation result demonstrates that CSMA is much closer to the optimal result than BSA, though standard deviation value of SMA is same as CSMA. The p-values for CSMA, SMA, and BSA are all less than 0.05 (nearly equal to zero), indicating that the data samples do not fit the normal distribution due to the rejection of H0 and acceptance of H1.

Table 7: One sample KS test results

| Parameters | BSA | SMA | CSMA |
| --- | --- | --- | --- |
| N | 30 | 30 | 30 |
| Mean | 1.9115 | 1.9200 | **1.9220** |
| SD | 0.003 | 0.0015 | 0.0015 |
| Most extreme differences | -0.0104 | -0.007 | -0.0065 |
| KSSTAT | 0.9715 | 0.9723 | 0.9726 |

Additionally, the paired t-test is used to explore differences between the algorithms. With a 0.05 significance level, $p$ value less than .05 implies that the mean of data sets is equal, whereas $p$ value more than .05 denotes that the mean of data sets is dissimilar. The test findings in Table 8 demonstrate that the three optimization algorithms are substantially different from one another, with paired p values less than 0.05. The standard deviation value proves that CSMA and SMA results are comparatively closer than the other pairs. Thus, from the other results depicted in Table 8, it can be concluded that the three pairs are considerably different to one another at 95% confidence level.

Table 8: Paired ttest results

| Parameter | BSA-CSMA | BSA-SMA | CSMA-SMA |
| --- | --- | --- | --- |
| Mean | -0.0103 | -0.0085 | 0.0018 |
| p | 0 | 0 | 0 |
| tstat | -14.2893 | -12.1661 | 4.2397 |
| SD | 0.0039 | 0.0038 | 0.0023 |

### 4.1.3 Optimal load shedding for Island-1

For simulation purposes, the performance at hour 16:00th is examined for all three island scenarios, with 100 % load demand and PVs operating at full capacity. The load demand at 16th hour is 1.4050 MW and total generation is 0.83 MW, representing a power mismatch of 40.9%. After completing optimization for Island-1, BSA has a fitness value of 1.9164, whilst SMA and CSMA achieves 1.9234 and 1.9265, respectively. The optimization procedure requires 52 seconds for SMA and 49 seconds for CSMA and BSA. It has been observed that CSMA has a higher fitness value

Figure 4.15: Buswise remaining load after optimization in Island-1
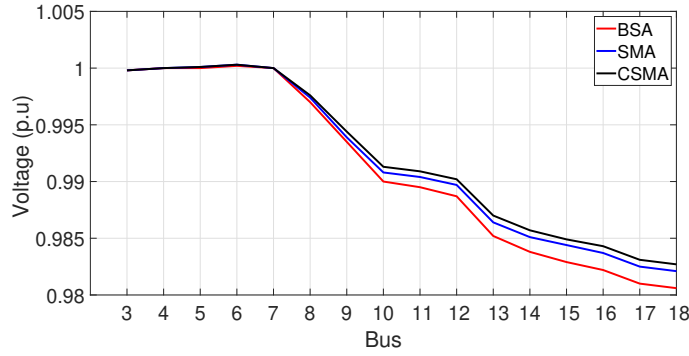


Figure 4.16: Voltage profile of Island-1 after optimization

than BSA and SMA and is faster in terms of computing time. After load shedding, BSA results in 0.822 MW of remaining load implying that 0.583 MW load is curtailed after optimization, whereas in the cases of SMA and CSMA, the remaining load is 0.823 MW and 0.824 MW. It has been found that CSMA curtails 2 kW and 1 kW less load than BSA and SMA, indicating CSMA's superior performance in maintaining the highest proportion of remaining load after optimum load shedding. Furthermore, CSMA distributes the remaining loads more evenly amongst the nodes of the network as shown in Figure 4.15, which makes the algorithm more coherent in terms of load shedding optimization.

Figure 4.16 illustrates the voltage profiles for all algorithms in Island-1 which demonstrates that CSMA also outperforms SMA and BSA in terms of voltage profiles. The voltage stability margin (VSM) of CSMA is 0.9334, while that of BSA and SMA is 0.925 and 0.9308, respectively. Hence, as far as voltage stability is concerned, which is an essential parameter in this study, CSMA is preferable to BSA and SMA.

### 4.1.4 Optimal load shedding for Island-2

Similar to Island-1, the simulations are done for the 16th hour with total load demand of 3.715 MW, while total generation is 1.83 MW with all the DG's operating. Following the application

of the optimal load shedding strategies discussed previously, the CSMA-based algorithm retains 1.8201 MW as remaining load, curtailing 1.8949 MW load from Island-2, whereas SMA and BSA , curtails 2.1 kW and 2.2 kW more than CSMA respectively as shown in Table 3. Similar to Island-1, CSMA outperforms SMA and BSA in determining the ideal amount of remaining load and ensuring voltage stability, as the primary goal of this study is to maximize the amount of load preserved. Figure 4.17 depicts the load remaining after optimization in kW at each bus for CSMA, SMA, and BSA, corresponding to the load priority limits considered.
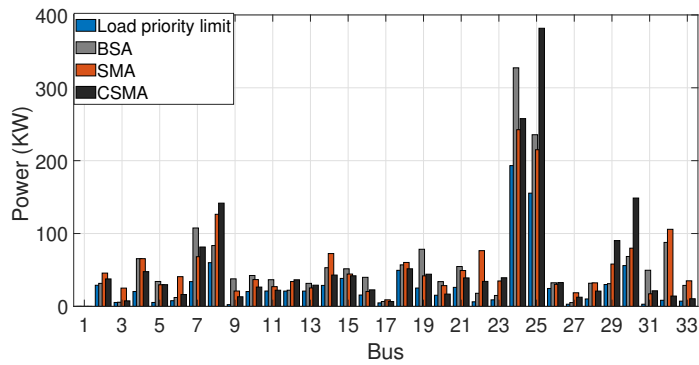


Figure 4.17: Buswise remaining load after optimization in Island-2
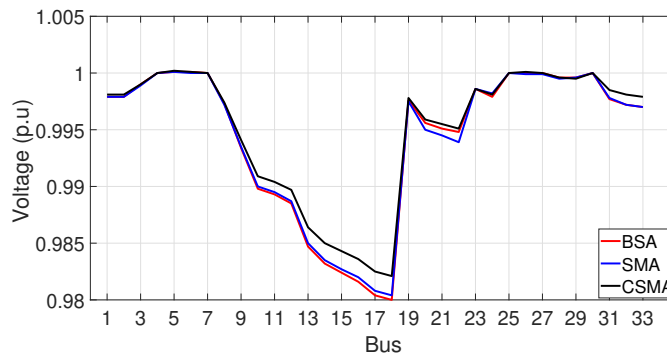


Figure 4.18: Voltage profile of Island-2 after optimization

CSMA-based algorithm exceeds SMA and BSA in terms of fitness value and VSM while requiring less computational time. Notably, the voltage stability indicator $VSM_{sys}$ value is significantly higher in CSMA, which makes the algorithm more efficient. Voltage profiles are also improved in the CSMA-based method, as seen in Figure 4.18. Though SMA or BSA provides superior results for particular buses, CSMA performs better in the overall circumstances with even distribution of the loads.

## 4.1.5 Optimal load shedding for Island-3

The optimization techniques are used for Island-3 in the same approach that they were used for Island-1 and Island-2. The mentioned island has a total demand of 2.674 MW and all the DG's
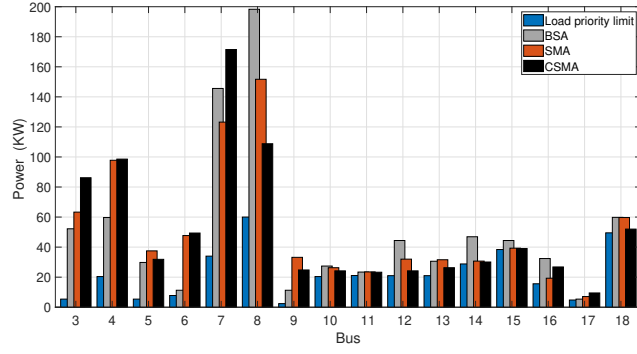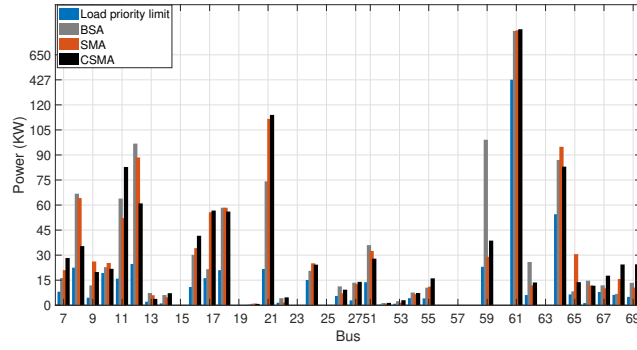
Figure 4.19: Buswise remaining load after optimization in Island-3
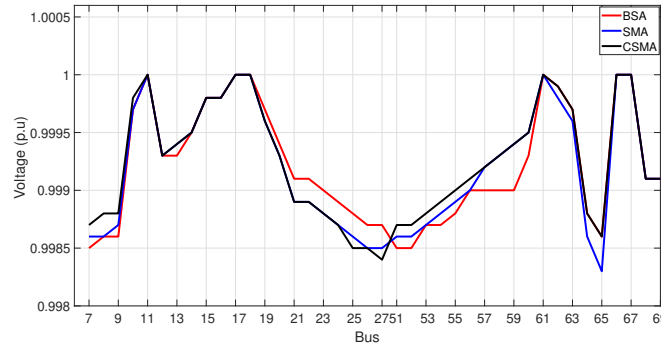


Figure 4.20: Voltage profile of Island-3 after optimization

total generation provides 1.747 MW with a power mismatch of 34.6%. The result indicates that CSMA outperforms SMA and BSA in terms of achieving the highest amount of remaining load after optimum load shedding. In addition, CSMA is quicker and has a higher fitness value than SMA and BSA. BSA provides a total of 1.715 MW load with less VSM value, whereas SMA and CSMA provide 13 kW and 20 kW more loads respectively to the networks as shown in Figure 4.19. Figure 4.20 depicts the voltage profiles of the buses after load shedding done by CSMA, SMA, and BSA. Though BSA provides superior voltage profiles for specific buses, CSMA provides the best overall performance including remaining load. After studying all three islanding scenarios, an intriguing conclusion can be drawn: as the size of the island network grows, the acceptability and performance of CSMA over SMA and BSA becomes more pronounced.

## 4.1.6 Convergence characteristics and hourly performance of CSMA

Figure 4.21 illustrates a 24-hour simulation of the proposed algorithm while maximizing the objective function. The figure indicates that the hourly performance of CSMA is quite impressive. It has been observed that, CSMA is efficient in utilizing the total power generation in an effective way by allocating optimal remaining loads throughout the network. Furthermore, the difference

between power generation and remaining load is minimal, indicating that the algorithm adequately utilizes the total power generation. Moreover, in terms of algorithm convergence characteristics, Figure 4.22 depicts Island-2's convergence curve for all the three algorithms. In addition, Figure 4.23 depicts a zoomed-in representation of the convergence curve, allowing each algorithm's differences of fitness values to be distinguished. As shown in the figure, CSMA converges faster than BSA and SMA, making the algorithm more suitable for load shedding optimization, as fast convergence characteristics of the algorithm is one of the most important criteria in load shedding optimization.
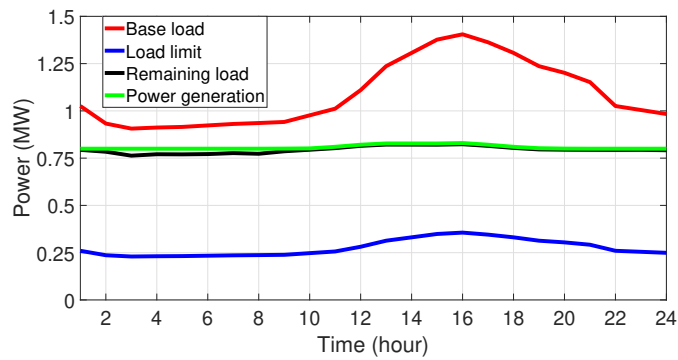


Figure 4.21: 24 hour basis CSMA performance on Island-1
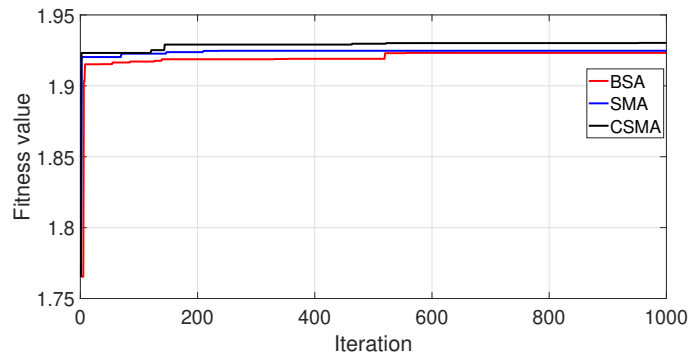


Figure 4.22: Convergence curve for Island-2
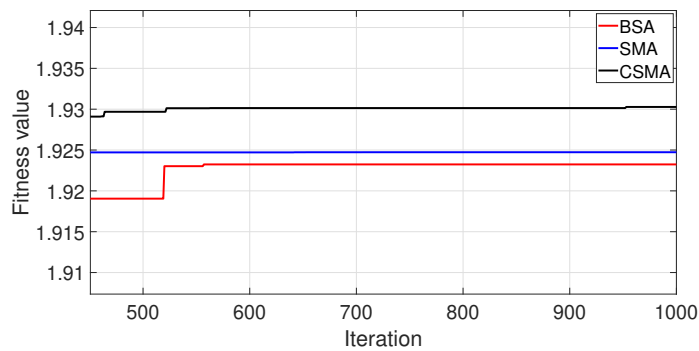


Figure 4.23: Zoomed version

42

## 4.2 Optimal Sizing and Placement of Multiple DG Units

In this work, IEEE 33 bus and 69 bus radial distribution systems are being used as test systems.To assess the efficacy of the suggested CEO algorithm, the system performances are evaluated and compared to TLBO, MMFO, and the original EO algorithm using MATLAB. The next section compares CEO, EO, MMFO, and TLBO in terms of overall computational time and fitness values achieved. To achieve a valid comparison, the initial population set size (50) and total iteration number (100) are kept identical for all the four algorithms. Furthermore, the algorithms' termination condition is set to the maximum number of iterations. Furthermore, each technique is evaluated 30 times for 3 and 4 DG penetration scenarios for nonparametric statistical analysis , with the best, mean and the worst outcomes presented.

### 4.2.1 Comparative analysis of the algorithms

Table 9 shows the best, average, and worst results of fitness values and elapsed time duration for independent 30 runs of each method in the case of 3 DG and 4 DG placement in IEEE 33 and 69 bus systems. It appears that, in terms of fitness value, CEO outperforms rest of the three algorithms. In some of the cases, worst fitness result of CEO is better than the best result of MMFO. Also it has been observed that, MMFO is faster than TLBO although TLBO performs better than MMFO in terms of fitness value. Moreover, EO and CEO beats TLBO by a fair margin regarding elapsed time as TLBO has the highest computational time among all the algorithms. Notably, CEO beats EO in terms of average, best, and worst fitness values, regardless of whether CEO outperforms EO by a small margin in terms of computing speed. Hence, it has been established that CEO trumps all other algorithms in both of fitness function value and computational speed.

### 4.2.2 Nonparametric statistical analysis

The non-parametric statistical analysis was conducted for 30 individual runs to better assess the performance of the aforementioned four methods. Following that, each method is subjected to the one-sample Kolmogorov–Smirnov (KS) test and the results are illustrated in Table 10. At a level of significance of 0.05, the null hypothesis, H0, indicates that the data are normally distributed, whereas the second hypothesis, H1, indicates that the data do not fit to a normal distribution.

It has been observed that, CEO outperforms TLBO, MMFO and EO for 3 DG and 4 DG placement scenarios of IEEE 33 and 69 bus radial distribution system in terms of mean value. Furthermore, the standard deviation (SD) values presented in the following table represents that CEO is significantly nearer to the optimal solution due to it's low SD value than TLBO, MMFO and EO. In addition, for all scenarios of DG placement, the most extreme difference is smallest for

Table 9: Comparative results

| System | DG | Parameter | Algorithm | Fitness | Elapsed Time(s) |
|--------|-----|-----------|-----------|---------|-----------------|
| 33 Bus | 3 DG | Best result | TLBO | 0.1779 | 19.4862 |
| | | | MMFO | 0.2432 | 9.4949 |
| | | | EO | 0.1772 | 8.0346 |
| | | | CEO | **0.1686** | **7.9545** |
| | | Average result | TLBO | 0.2125 | 19.9466 |
| | | | MMFO | 0.2572 | 8.5760 |
| | | | EO | 0.1918 | 8.7512 |
| | | | CEO | **0.1831** | **8.6425** |
| | | Worst result | TLBO | 0.2444 | 21.1554 |
| | | | MMFO | 0.3065 | 9.4782 |
| | | | EO | 0.2383 | 9.9108 |
| | | | CEO | **0.2295** | **9.8609** |
| | 4 DG | Best result | TLBO | 0.1185 | 18.6736 |
| | | | MMFO | 0.1254 | 8.9809 |
| | | | EO | 0.1196 | 8.3477 |
| | | | CEO | **0.1149** | **8.0447** |
| | | Average result | TLBO | 0.1321 | 20.5070 |
| | | | MMFO | 0.1898 | 8.9374 |
| | | | EO | 0.1343 | 9.1064 |
| | | | CEO | **0.1242** | **8.7730** |
| | | Worst result | TLBO | 0.1740 | 25.1213 |
| | | | MMFO | 0.2431 | 9.4153 |
| | | | EO | 0.1630 | 10.0943 |
| | | | CEO | **0.1323** | **9.2473** |
| 69 Bus | 3 DG | Best result | TLBO | 0.1579 | 45.8670 |
| | | | MMFO | 0.1802 | 19.0329 |
| | | | EO | 0.1454 | 19.4216 |
| | | | CEO | **0.1441** | **18.7133** |
| | | Average result | TLBO | 0.1649 | 50.8927 |
| | | | MMFO | 0.2437 | 21.1875 |
| | | | EO | 0.1593 | 21.5526 |
| | | | CEO | **0.1528** | **21.0240** |
| | | Worst result | TLBO | 0.1884 | 55.7464 |
| | | | MMFO | 0.3622 | 22.9471 |
| | | | EO | 0.1901 | 23.1049 |
| | | | CEO | **0.1706** | **22.3797** |
| | 4 DG | Best result | TLBO | 0.0957 | 46.3230 |
| | | | MMFO | 0.1255 | 19.7123 |
| | | | EO | 0.1094 | 19.0122 |
| | | | CEO | **0.0927** | **18.6655** |
| | | Average result | TLBO | 0.1198 | 50.6832 |
| | | | MMFO | 0.2077 | 21.7933 |
| | | | EO | 0.1368 | 22.4092 |
| | | | CEO | **0.1160** | **22.4059** |
| | | Worst result | TLBO | 0.1540 | 58.0237 |
| | | | MMFO | 0.2667 | 23.3013 |
| | | | EO | 0.1901 | 23.2928 |
| | | | CEO | **0.1427** | **26.4638** |

CEO.

The paired t-test is also utilized to investigate discrepancies of the algorithms and results are shown in Table 11. With a level of significance of 0.05, $p$ value lesser than 0.05 indicates that the average of the data sets is identical, however a $p$ value greater than 0.05 indicates that the average of the data sets is different. It has been observed that, TLBO and EO results are closer for the 4 DG case of the IEEE 33 bus and 3 DG case of the IEEE 69 bus system, while TLBO and CEO are

Table 10: KS test results (One sample)

| System | DG | Parameters | TLBO | MMFO | EO | CEO |
|--------|-----|------------|------|------|-----|-----|
| 33 bus | 3 DG | N | 30 | 30 | 30 | 30 |
| | | Mean | 0.2125 | 0.2572 | 0.1918 | 0.1831 |
| | | SD | 0.0208 | 0.0139 | 0.0178 | 0.0097 |
| | | Most extreme difference | -0.0665 | -0.0632 | -0.0611 | -0.0609 |
| | | KSStat | 0.5706 | 0.5961 | 0.5703 | 0.5669 |
| | 4 DG | N | 30 | 30 | 30 | 30 |
| | | Mean | 0.1321 | 0.1898 | 0.1343 | 0.1242 |
| | | SD | 0.0119 | 0.0287 | 0.0117 | 0.0051 |
| | | Most extreme difference | -0.0555 | -0.1177 | -0.0434 | -0.0174 |
| | | KS stat | 0.5472 | 0.5499 | 0.5476 | 0.5457 |
| 69 bus | 3 DG | N | 30 | 30 | 30 | 30 |
| | | Mean | 0.1649 | 0.2437 | 0.1593 | 0.1528 |
| | | SD | 0.0073 | 0.0441 | 0.0111 | 0.0073 |
| | | Most extreme difference | -0.0305 | -0.1820 | -0.0447 | -0.0265 |
| | | KS stat | 0.5627 | 0.5715 | 0.5578 | 0.5573 |
| | 4 DG | N | 30 | 30 | 30 | 30 |
| | | Mean | 0.1198 | 0.2077 | 0.1368 | 0.1160 |
| | | SD | 0.0138 | 0.0395 | 0.0190 | 0.0103 |
| | | Most extreme difference | -0.0583 | -0.1412 | -0.0807 | -0.0500 |
| | | KS stat | 0.5381 | 0.5499 | 0.5435 | 0.5369 |

Table 11: Paired ttest result

| System | DG | Case | Mean | p | tstat | SD |
|--------|-----|------|------|-----|-------|-----|
| 33 bus | 3 DG | TLBO-MMFO | -0.0448 | 1.4310e-11 | -10.6871 | 0.0230 |
| | | TLBO-EO | 0.0206 | 0.0010 | 3.6542 | 0.0309 |
| | | TLBO-CEO | 0.0294 | 4.6143e-08 | 7.3195 | 0.0220 |
| | | MMFO-EO | 0.0654 | 2.2091e-14 | 13.9351 | 0.0257 |
| | | MMFO-CEO | 0.0741 | 5.5520e-20 | 22.6409 | 0.0179 |
| | | EO-CEO | 0.0087 | 0.0360 | 2.1992 | 0.0218 |
| | 4 DG | TLBO-MMFO | -0.0577 | 1.1532e-11 | -10.7863 | 0.0293 |
| | | TLBO-EO | -0.0023 | 0.4465 | -0.7718 | 0.0160 |
| | | TLBO-CEO | 0.0079 | 0.0021 | 3.3716 | 0.0128 |
| | | MMFO-EO | 0.0555 | 1.9886e-11 | 10.5369 | 0.0288 |
| | | MMFO-CEO | 0.0656 | 3.4541e-13 | 12.4829 | 0.0288 |
| | | EO-CEO | 0.0101 | 7.2931e-04 | 3.7776 | 0.0147 |
| 69bus | 3 DG | TLBO-MMFO | -0.0787 | 1.0850e-10 | -9.7823 | 0.0441 |
| | | TLBO-EO | 0.0056 | 0.0403 | 2.1468 | 0.0143 |
| | | TLBO-CEO | 0.0120 | 1.6243e-06 | 5.9929 | 0.0110 |
| | | MMFO-EO | 0.0843 | 1.0066e-10 | 9.8149 | 0.0471 |
| | | MMFO-CEO | 0.0907 | 6.8267e-12 | 11.0297 | 0.0451 |
| | | EO-CEO | 0.0064 | 0.0289 | 2.2991 | 0.0152 |
| | 4 DG | TLBO-MMFO | -0.0879 | 7.9853e-13 | -12.0625 | 0.0399 |
| | | TLBO-EO | -0.0169 | 0.0014 | -3.5333 | 0.0262 |
| | | TLBO-CEO | 0.0038 | 0.2870 | 1.0847 | 0.0193 |
| | | MMFO-EO | 0.0709 | 2.7574e-09 | 8.4262 | 0.0461 |
| | | MMFO-CEO | 0.0917 | 1.1704e-13 | 13.0407 | 0.0385 |
| | | EO-CEO | 0.0207 | 1.9416e-06 | 5.9279 | 0.0192 |

comparable for the 4 DG case of the IEEE 69 bus system. Furthermore, the remaining pairings have $p$ values less than 0.05, indicating that they are significantly different from one another.
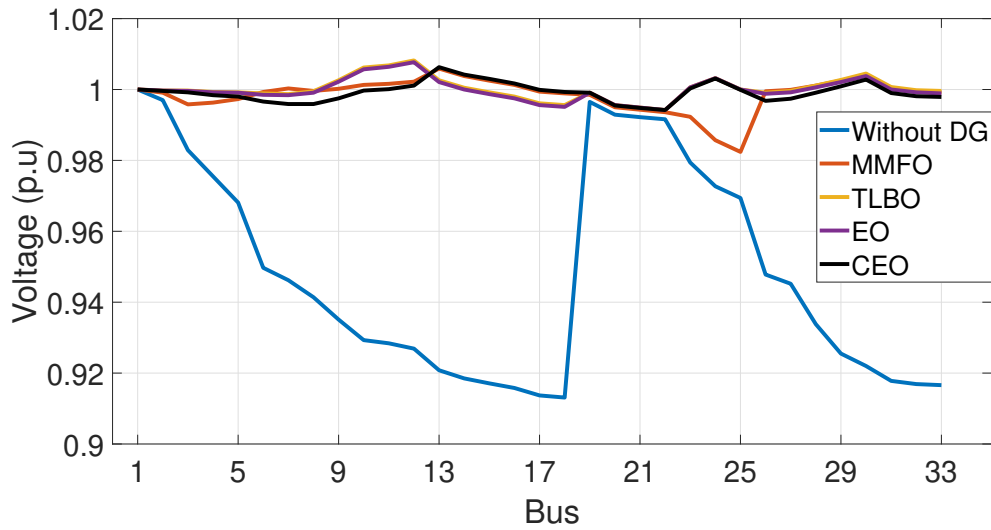
'

(a) Voltage profile for IEEE 33 bus system
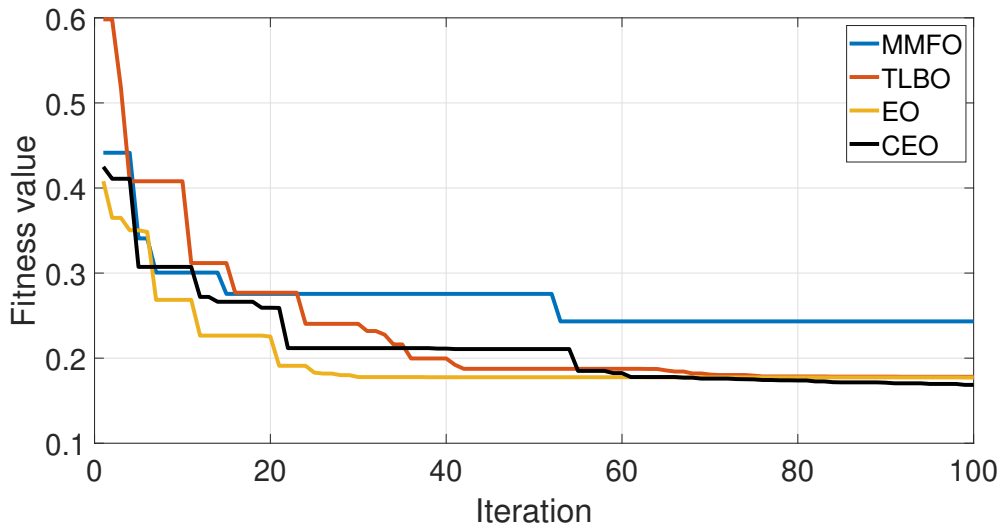


(b) Convergence curve for IEEE 33 bus system

Figure 4.24: Three DG units installation

### 4.2.3 Three DG units

The CEO simulation results are compared to other techniques for locating and sizing three DG units in Table 12. Particularly, for demonstration purposes, only the best result out of the 30 independent runs are presented here for each algorithm. In terms of reducing power loss and voltage deviation, it appears that the suggested CEO algorithm outperforms all other algorithms evaluated when three DG units are used in IEEE 33 bus systen. It has also been observed that, for 33 bus system, CEO minimizes the active power loss by 90.3% to the base loss, which is the best of all the algorithms compared. Furthermore, CEO provides 0.7% , 4.5% and 0.8% less power loss compared to EO, MMFO and TLBO. Similarly, in the IEEE 69 bus system, CEO reduces active power loss to the base loss by 92.7%, which remains the superior of all the algorithms.

Table 12: Results obtained for three DG units installation

| System | Algorithm | DG 1 | | DG 2 | | DG 3 | | Loss (kW) | Voltage Deviation | Fitness | Elapsed Time (s) |
|--------|-----------|------|-----|------|-----|------|-----|-----------|-------------------|---------|------------------|
| | | Size(MVA) | Bus | Size(MVA) | Bus | Size(MVA) | Bus | | | | |
| 33 Bus | TLBO | 1.1428 | 12 | 1.3028 | 24 | 1.4307 | 30 | 21.1 | 0.0739 | 0.1780 | 19.4862 |
| | MMFO | 0.8218 | 13 | 1.3942 | 30 | 0.7205 | 7 | 28.7 | 0.1015 | 0.2432 | 9.4949 |
| | EO | 1.1365 | 12 | 1.4148 | 30 | 1.3108 | 24 | 20.9 | 0.074 | 0.1772 | 8.0346 |
| | CEO | 1.3438 | 24 | 1.4579 | 30 | 0.9581 | 13 | 19.6 | 0.0718 | **0.1685** | **7.9545** |
| 69 Bus | TLBO | 0.9299 | 57 | 1.4346 | 63 | 0.8293 | 14 | 19.4 | 0.0699 | 0.1579 | 45.8670 |
| | MMFO | 0.8331 | 14 | 1.0165 | 58 | 1.234 | 64 | 21.3 | 0.0835 | 0.1801 | 19.0329 |
| | EO | 0.9701 | 63 | 1.1154 | 13 | 1.0512 | 61 | 16.1 | 0.0723 | 0.1453 | 19.4216 |
| | CEO | 1.0801 | 61 | 0.8821 | 14 | 1.0029 | 62 | 14.1 | 0.0801 | **0.1441** | **18.7133** |

Table 13: Results obtained for four DG units installation

| System | Algorithm | DG 1 | | DG 2 | | DG 3 | | DG 4 | | Loss(kW) | Voltage Deviation | Fitness | Elapsed Time (s) |
|--------|-----------|------|-----|------|-----|------|-----|------|-----|----------|-------------------|---------|------------------|
| | | Size(MVA) | Bus | Size(MVA) | Bus | Size(MVA) | Bus | Size(MVA) | Bus | | | | |
| 33 Bus | TLBO | 0.6089 | 15 | 1.1176 | 7 | 1.0157 | 24 | 1.0362 | 31 | 14.1 | 0.0489 | 0.1185 | 18.6764 |
| | MMFO | 1.052 | 24 | 0.9789 | 6 | 1.2342 | 30 | 0.646 | 14 | 14.1 | 0.0558 | 0.1254 | 8.9800 |
| | EO | 1.0252 | 25 | 1.2383 | 30 | 0.9247 | 8 | 0.5371 | 15 | 14.5 | 0.048 | 0.1196 | 8.3477 |
| | CEO | 1.2333 | 30 | 0.8036 | 7 | 1.1388 | 24 | 0.6477 | 15 | 13.6 | 0.0477 | **0.1140** | **8.0447** |
| 69 Bus | TLBO | 1.0777 | 62 | 0.4004 | 20 | 0.955 | 61 | 0.7515 | 67 | 10.4 | 0.0485 | 0.0960 | 46.3230 |
| | MMFO | 1.2965 | 61 | 0.2838 | 23 | 1.04 | 66 | 0.6586 | 62 | 12 | 0.071 | 0.1254 | 19.7123 |
| | EO | 0.562 | 17 | 1.1037 | 61 | 0.8985 | 62 | 0.7504 | 51 | 10.7 | 0.0608 | 0.1093 | 19.0122 |
| | CEO | 0.9434 | 62 | 1.0488 | 61 | 0.9095 | 10 | 0.3636 | 23 | 10.4 | 0.0455 | **0.0926** | **18.6655** |

Moreover, CEO generates the best fitness value of all the algorithms in the 69 bus system. It has also been observed that, for both the systems, CEO is the fastest of all the algorithms in terms of computational time. Moreover, as seen in Figure 3.9b, CEO and EO converge significantly faster than TLBO and MMFO for 69 bus system. Figures 4.24a depict the effect of adding three DG units on the voltage profile while utilizing the considered algorithms. As indicated, CEO appears to provide the optimal voltage profile for the 33 bus system. However, for 69 bus systems, TLBO outperforms CEO in terms of voltage profile, but CEO remains the best approach due to greater fitness value, 3 kW less active power loss, and faster computational time.

## 4.2.4   Four DG units

Table 13 compares the CEO simulation results to different approaches for locating and sizing four DG units. Notably, only the best result of 30 separate runs for each algorithm are presented for illustrative purposes. In order to minimize power loss and voltage deviation, the suggested CEO algorithm appears to outperform rest of the algorithms investigated when using four DG units, as it does with three DG units. According to the findings obtained for both the test systems, CEO has the best fitness value and the shortest computing time, demonstrating the algorithm's superiority over alternative optimization methodologies. For 33 bus system, CEO reduces active power loss by 93.2% relative to the base loss, which is the best of all the algorithms tested. Furthermore, when compared to EO, MMFO, and TLBO, CEO delivers 0.9 KW, 0.5 KW, and 0.5 KW less power loss.

Additionally, CEO minimizes active power loss to base loss by 95.2 % in the IEEE 69 bus system, which is superior compared to the other methods tested. Furthermore, among the algorithms for each test system, the voltage deviation value for CEO was found to be the lowest. For the 69 bus system, however, CEO and TLBO both have the same amount of active power loss, but CEO has a significantly higher overall fitness value because of it's lower voltage deviation. In terms of computational time, CEO has been found to be the quickest of all the algorithms for both systems. In terms of convergence, CEO converges substantially earlier than EO, TLBO, and MMFO for each of the systems, as shown in Figure 4.25b. Moreover, Figures 4.25a shows the impact of using the suggested CEO for adding four DG units to the voltage profile. As illustrated, CEO appears to provide the optimal voltage profile for each test system, which makes the algorithm more efficient for optimal DG sizing and placement.

## 4.2.5 Optimal Load shedding

The suggested optimal load shedding methodology, which employs the chaotic equilibrium optimizer (CEO), is evaluated and compared with the original EO, BSA, and GOA. A comparative analysis of CEO, EO, BSA and GOA in terms of computational speed and fitness function values is demonstrated in the next section. To achieve a valid comparison,, the total iterations (300) and initial population set size (50) are kept identical for all the four algorithms. Furthermore, the algorithms' stopping criterion is the maximum number of iterations.

Table 14: Fitness values and corresponding elapsed time

| Algorithm | Parameter | 33 Bus | 69 Bus |
|-----------|-----------|--------|--------|
| BSA | Fitness Value | 1.7561 | 1.7225 |
|  | Remaining load (MVA) | 2.5058 | 2.0217 |
|  | VSM | 0.9856 | 0.9945 |
|  | Elapsed time (s) | 25.7916 | 64.9805 |
| GOA | Fitness Value | 1.8667 | 1.7615 |
|  | Remaining load (MVA) | 2.7914 | 2.1375 |
|  | VSM | 0.9827 | 0.9918 |
|  | Elapsed time(s) | 70.7301 | 166.6762 |
| EO | Fitness Value | 1.8700 | 1.9710 |
|  | Remaining load (MVA) | 2.7932 | 2.7375 |
|  | VSM | 0.9864 | 0.9853 |
|  | Elapsed time (s) | 23.5935 | 55.7042 |
| CEO | Fitness Value | **1.8802** | **1.9801** |
|  | Remaining load (MVA) | 2.8023 | 2.7492 |
|  | VSM | 0.9917 | 0.9896 |
|  | Elapsed time (s) | 23.6989 | 53.6316 |

Optimal load shedding for 33 Bus

The island of IEEE-33 bus was obtained by tripping the main generator from the grid and connecting it with 2 DGs obtained from CEO with optimal DG placement. The simulations are
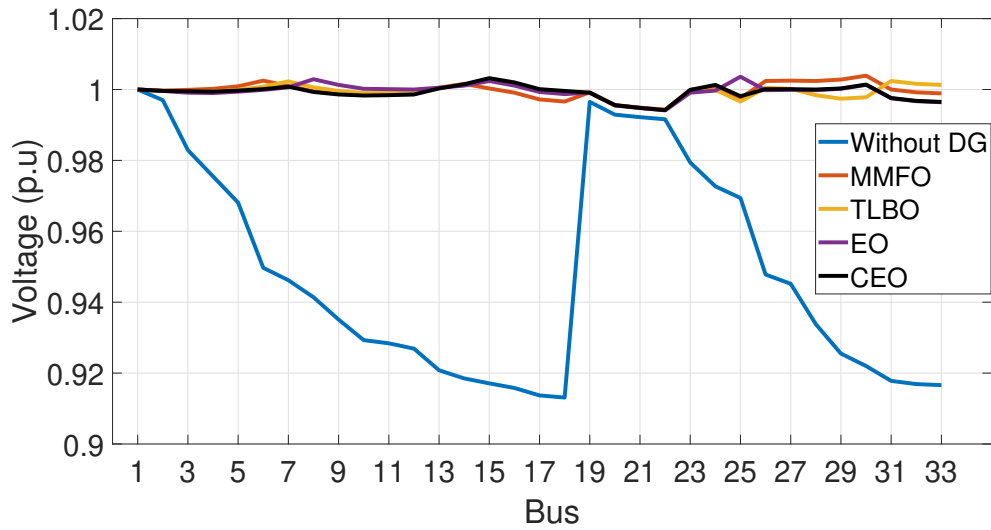
(a) Voltage profile for IEEE 33 bus system
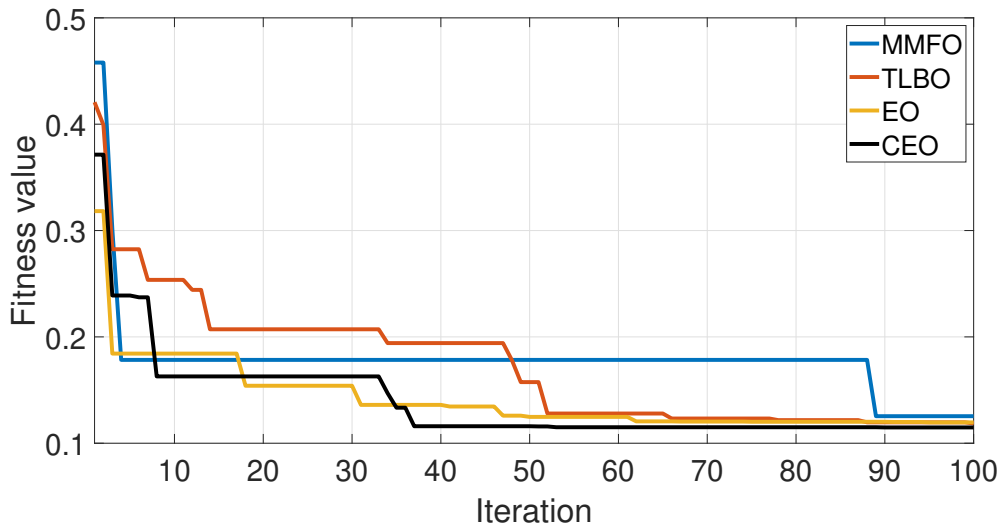


(b) Convergence curve for IEEE 33 bus system

Figure 4.25: Four DG units installation

done for 100% load level with the total load demand being 4.369 MVA, while the total power generation is 2.847 MVA with DG 1 (1.3678 MVA) operating at $10^{\text{th}}$ bus and DG 2 (1.48 MVA) operating at the $30^{\text{th}}$ bus. According to the results obtained , the CEO-based algorithm retains 2.802 MVA as remaining apparent load, curtailing 1.567 MVA load , whereas BSA, GOA, and EO curtails 296.5 kVA, 10.9 kVA, and 9.1 kVA more than CEO respectively as shown in Table 14. As the key objective of this part of the work is to maximize the amount of remaining load, it appears that CEO outperforms GOA, EO, and BSA while calculating the optimal quantity of remaining load and preserving voltage stability. Figure 4.26b depicts the remaining load after optimization throughout the network for CEO, EO, GOA and BSA, according to the load priority limits for each bus. Regarding fitness value and VSM, the CEO-based approach outperforms the other algorithms

while needing less computing time. Moreover, the $VSM_{sys}$ value in CEO is significantly greater. Voltage profile of the network has also enhanced in the CEO-based approach, as shown in Figure 4.26a. Moreover Figure 4.26c depicts convergence curve for all four approaches. CEO converges considerably faster, as illustrated in the figure, making the algorithm more convenient in terms of optimal load shedding.

Optimal load shedding for 69 Bus

Similar to the 33-bus system, the island of IEEE-69 bus was obtained by tripping the main generator from the grid and connecting it with 2 DGs obtained from CEO with optimal DG placement. The simulations are done for 100% load level with total load demand of 4.66 MVA (3.802 MW and 2.695 MVAr ), while total generation is 2.777 MVA with DG 1 (1.2977 MVA) placed at $13^{th}$ bus and DG2 (1.48 MVA) placed at the $64^{th}$ bus. After optimization, CEO has a fitness value of 1.9801, whereas BSA, GOA, and EO have fitness values of 1.7225, 1.7615, and 1.9710, respectively. CEO has a greater fitness value than the other algorithms and is quicker in terms of computational time. It has been observed that BSA results in 2.021 MVA of remaining apparent load, implying that 56.6 % of the total load is shed during optimization, whether in the instances of GOA, EO, and CEO, the total remaining load is 2.1375 MVA, 2.7375 MVA, and 2.7492 MVA, respectively, corresponding to 54.2%, 41.3%, and 41% load shedding. According to the findings, CEO offers 11.7 kVA, 611.7 kVA, and 727.6 kVA more remaining load than EO, GOA, and BSA, demonstrating CEO's better results in preserving the maximum portion of total remaining load after optimization. Furthermore, as illustrated in Figure 4.27b, CEO allocates the remaining loads more equitably throughout the buses. Figure 4.27c depicts convergence curve of the algorithms and similarly to the 33 bus system CEO converges considerably faster. The voltage profile of the algorithms are depicted in Figure 4.27a. In addition, CEO has a voltage stability margin (VSM) of 0.9896, whereas BSA, GOA, and EO have VSMs of 0.9935, 0.9918, and 0.9853, respectively.

## 4.3 Optimal Planning of Multiple Renewable Energy-Integrated Distribution System with Uncertainties

IEEE 33 bus and 69 bus radial distribution systems are employed as test systems in this work. The flowchart of the algorithm is depicted in Fig. 4.29. The system performances are analyzed and compared to HHO-PSO and the PPSOGSA algorithms using MATLAB software to analyze the efficiency of the proposed AHA algorithm. The Newton-Raphson power flow method is adopted in this study. In addition, two types of simulations were investigated to check the validity of the proposed algorithm. Firstly, optimal RDG sizing and placement problem are simulated by

Table 15: IEEE 33 bus optimal size and location of RDG farms

| Algorithm | Farm | Location bus | $N_{RDG}$ | $P_{RDGF}$ |
|-----------|------|--------------|-----------|------------|
| PPSOGSA   | PV   | 13           | 5         | 1          |
|           | WT   | 29           | 9         | 1.8        |
| HH0-PSO   | PV   | 33           | 8         | 1.6        |
|           | WT   | 13           | 5         | 1          |
| AHA       | PV   | 11           | 7         | 1.4        |
|           | WT   | 6            | 6         | 1.2        |

Table 16: IEEE 33 bus optimised results of economical and technical metrics for ten years

| Index             | PPSOGSA   | HHO-PSO   | AHA           |
|-------------------|-----------|-----------|---------------|
| Energy loss (MWh) | 8074.1245 | 9539.465  | **7700.4135** |
| Average $V_D$     | 0.096     | 0.14      | **0.093**     |
| Average VSM       | 0.921     | 0.912     | 0.932         |
| TAES              | 591969.3  | 518682.64 | **610682.342**|

considering the effect of uncertainties in RDG generation and seasonal load profiles. Secondly, under a constant power load, ideal RDG size and location are simulated without considering uncertainties. To provide a valid comparison, the initial population set size (50) and total iteration number (100) for all three algorithms are maintained constant. Furthermore, the termination condition of the algorithms is set to the maximum number of iterations.

Table 17: IEEE 69 bus optimal size and location of RDG farms

| Algorithm | Farm | Location bus | $N_{RDG}$ | $P_{RDGF}$ |
|-----------|------|--------------|-----------|------------|
| PPSOGSA   | PV   | 61           | 9         | 1.8        |
|           | WT   | 13           | 5         | 1          |
| HH0-PSO   | PV   | 61           | 9         | 1.8        |
|           | WT   | 69           | 6         | 1.2        |
| AHA       | PV   | 61           | 9         | 1.8        |
|           | WT   | 17           | 3         | 0.6        |

## 4.3.1 RDG Sizing and Placement Considering Uncertainties

The objective is to achieve the optimum size and location for one WT farm and one PV farm in the IEEE 33 and 69-bus system. For both WT and PV generation, $P_{RDGi}$ is set as 200 kW with unity power factor, while $NRDGi_{max}$ is chosen as 10.

The wind speed and solar irradiation measurements originate from [94], which are recorded with a sample period of 5 minutes for the whole year of 2016. The year is considered to be divided into three seasons: spring (August, September, and October), summer (March, April, May, June, and July), and winter (November, December, January and February). The mean values and standard deviations of wind speed and solar irradiation are determined for each hour of a typical day based on the collected data, which was further utilized to generate the discrete PDFs of wind speed and

Table 18: IEEE 69 bus optimised results of economical and technical metrics for ten years

| Index | PPSOGSA | HHOPSO | AHA |
|---|---|---|---|
| Energy loss (MWh) | 5585.996 | 6018.714 | **5241.7885** |
| Average VD | 0.0639 | 0.1125 | **0.0622** |
| Average VSM | 0.951 | 0.933 | **0.958** |
| TAES | 803566.442 | 782101.18 | **821007.1** |

Table 19: Input parameters for RDG sizing and placement without considering uncertainties

| Parameter | Value |
|---|---|
| $N_{iter,max}$ | 100 |
| $N_{pop}$ | 50 |
| $N_{runs}$ | 50 |
| Bus voltage limits (p.u.) | $\pm 5\%$ |
| RDG size limits (MVA) | $0 \leq S_{DG,max} \leq 2$ |
| Total generation (MVA) | $\sum_{m=1}^{N_{DG}} S_{DG,m} \leq 3$ |
| RDG PF limits | $pf_{PV}=1$ & $0.65 \leq pf_{WT} \leq 1$ |
| $C_{DG}$ ($/kW$) | 30 |
| $T_{DG}$ (years) | 10 |
| $C_E$ ($/kWh$) | 0.05 |
| $R(\%)$ | 10 |

solar irradiance for each hour. Using typical day patterns for seasons, the projected power of WT and PV is evaluated for each year over a 10-year planning horizon. Table 15 shows the optimal size and location of RDG farms on the IEEE 33 bus using the three algorithms.

Table 16 illustrates the optimized outcomes of economic and technical metrics throughout a ten-year period. As compared to PPSOGSA and HHO-PSO, AHA yields 5.3% and 26% reduced energy losses. Furthermore, AHA outperforms PPSOGSA and HHO-PSO in terms of average voltage deviation ($V_D$) for each hour by 3.2% and 50.5%, respectively. In addition, as compared to the other algorithms, AHA achieved the maximum $VSM_{sys}$ and overall energy savings value. Besides, AHA appears to require the fewest amount of elementary RDGs while still providing the optimum solution. The findings are compared with AHA results for demonstration purposes and presented in a bar diagram in Fig. 4.28.

Table 17 shows the optimal size and placement of RDG farms using the three methods for the IEEE 69 bus system. Table 18 presents the optimized outcomes of economic and technical metrics throughout a ten-year period. In comparison to PPSOGSA and HHO-PSO, AHA delivers 6.5% and 14.8% reduced energy losses, respectively. Besides, AHA employs the fewest number of elementary RDGs. Additionally, AHA's average voltage deviation ($VD$) for each hour is 2.7% lower and 80.8% lower than that of PPSOGSA and HHO-PSO, respectively. Furthermore, AHA outperforms all the other algorithms in terms of $VSM_{sys}$ and overall energy savings. In a bar diagram, Fig. 19 illustrates the findings compared in percentage with respect to AHA.

Table 20: IEEE 33 bus optimal results for RDG placement without uncertainties

| Case | Algorithm | Optimal result | | | Loss (kW) | Deviation | VSM | TAES |
|------|-----------|------|-----------|------|-----------|-----------|-----|------|
| | | Bus | Size (MVA) | p.f. | | | | |
| 2 PV | HHO PSO | 32 | 1.5273, | 1 | 135.3 | 0.2863 | 0.9355 | 29420.13 |
| | | 18 | 1.2363 | 1 | | | | |
| | PSO PGA | 32 | 1.6524 | 1 | 123.2 | 0.1808 | 0.9396 | 34724.09 |
| | | 13 | 1.3476 | 1 | | | | |
| | AHA | 13 | 1.3421 | 1 | **119.5** | **0.174** | **0.9398** | **36338.3** |
| | | 31 | 1.6577 | 1 | | | | |
| 3 PV | HHO PSO | 32 | | 1 | 111.9 | 0.2601 | 0.9351 | 39691 |
| | | 13 | 0.2417 | 1 | | | | |
| | | 33 | 1.25211.2323 | 1 | | | | |
| | PSO PGA | 15 | 1.65234 | 1 | 114.4 | 0.1896 | 0.9414 | 38600.06 |
| | | 31 | 1.5644 | 1 | | | | |
| | | 28 | 0.4132 | 1 | | | | |
| | AHA | 10 | 0.8607 | 1 | **111.1** | **0.1594** | **0.9393** | **40010.3** |
| | | 32 | 1.5285 | 1 | | | | |
| | | 16 | 0.609 | 1 | | | | |
| 2 WT | HHO PSO | 12 | 0.8873 | 0.7352 | 63.9 | 0.2715 | 0.9462 | 60860.957 |
| | | 33 | 1.9953 | 0.8791 | | | | |
| | PSO PGA | 30 | 1.5849 | 0.9671 | 53.3 | 0.1344 | 0.945 | 64677.555 |
| | | 11 | 1.361 | 0.9499 | | | | |
| | AHA | 29 | 1.7785 | 0.9315 | **46.8** | **0.1312** | **0.947** | **68378.5** |
| | | 12 | 1.1715 | 0.9403 | | | | |
| 3 WT | HHO PSO | 11 | 1.8961 | 0.95 | 59.7 | 0.2679 | 0.9393 | 62530 |
| | | 19 | 0.2196 | 0.6516 | | | | |
| | | 32 | 0.8653 | 0.9284 | | | | |
| | PSO PGA | 29 | 1.8383 | 0.8497 | 35.4 | 01548 | 0.9253 | 73200 |
| | | 6 | 0.1166 | 0.9767 | | | | |
| | | 12 | 0.9686 | 0.9123 | | | | |
| | AHA | 8 | 0.9836 | 0.9094 | **30.3** | **0.0993** | **0.9171** | **75426.2** |
| | | 29 | 1.5377 | 0.8843 | | | | |
| | | 16 | 0.4739 | 0.8625 | | | | |

## 4.3.2 RDG Sizing and Placement Without Considering Uncertainties

To validate the suggested algorithm's efficiency in contrast to previous optimization techniques, the problem of RDG sizing and placement for dispatchable RDG units is investigated. Multiple PV and WT penetration levels are simulated and assessed. The PV induces solely active power, whereas the WT can accommodate both active and reactive power. Furthermore, it is anticipated that only one RDG unit can be penetrated on the same bus at a time. A potential solution set, for example, can be represented as a vector composed of three variables such as PV/WT locations, size, and the power factor of RDG units at these locations. The first variable determines the placement of RDGs on network buses. The second variable represents the power generation of RDGs at the given load level, with actual values ranging from 0 to the maximum capacity of the related RDG. Each of the third variable has a value ranging from 0 to 1 and indicates the optimal power factor of the installed WT-DG units. However, when PV-type DG units are installed, the values of that variable are always 1. Besides, it has been assumed that the load model is constant and PV's and WT's generation is not affected by natural uncertainties. The fundamental purpose of the optimization is to identify the most appropriate size and location of RDGs in order to improve the distribution system's techno-economic efficiency.

Table 19 displays the input data and cost parameters for the optimum planning problem. Two scenarios of RDG integration, including two and three PV/WTs, are investigated to demonstrate the beneficial impacts of appropriate allocation on system performance. Table 20 compares the

Table 21: IEEE 69 bus optimal results for RDG placement without uncertainties

| Case | Algorithm | Optimal result | | | Loss (kW) | Deviation | VSM | TAES |
|------|-----------|------|-----------|------|-----------|-----------|------|------|
| | | Bus | Size (MVA) | p.f. | | | | |
| 2 PV | HHO PSO | 65 | 1.7056 | 1 | 108.7 | 0.2604 | 0.977 | 48872.69 |
| | | 13 | 1.2327 | 1 | | | | |
| | PSO PGA | 65 | 1.69 | 1 | 110.1 | 0.2391 | 0.977 | 48255.15 |
| | | 13 | 1.31 | 1 | | | | |
| | AHA | 14 | 0.9827 | 1 | **95.1** | **0.177** | **0.977** | **54845.48** |
| | | 64 | 1.9862 | 1 | | | | |
| 3 PV | HHO PSO | 68 | 1.0746 | 1 | 103.6 | 0.2999 | 0.977 | 51111.28 |
| | | 27 | 0.3007 | 1 | | | | |
| | | 65 | 1.6229 | 1 | | | | |
| | PSO PGA | 65 | 1.0443 | 1 | 92.7 | 0.1528 | 0.9733 | 55887.59 |
| | | 60 | 1.3383 | 1 | | | | |
| | | 23 | 0.6172 | 1 | | | | |
| | AHA | 19 | 0.6833 | 1 | **91.2** | **0.1307** | **0.9758** | **60934.07** |
| | | 64 | 0.4941 | 1 | | | | |
| | | 61 | 1.792 | 1 | | | | |
| 2 WT | HHO PSO | 64 | 1.8665 | 0.9809 | 59.6 | 0.3317 | 0.9771 | 70370.8863 |
| | | 20 | 0.9951 | 0.9756 | | | | |
| | PSO PGA | 15 | 0.7282 | 0.8687 | 23.7 | 0.152 | 0.9722 | 86089.27 |
| | | 64 | 1.9971 | 0.784 | | | | |
| | AHA | 14 | 0.9937 | 0.6746 | **18.7** | **0.0906** | **0.9772** | **88298.91** |
| | | 63 | 1.9984 | 0.8991 | | | | |
| 3 WT | HHO PSO | 46 | 0.3136 | 0.9201 | 70.7 | 0.2679 | 0.959 | 65527.04 |
| | | 65 | 1.3817 | 0.9746 | | | | |
| | | 27 | 0.8725 | 0.8119 | | | | |
| | PSO PGA | 65 | 1.9565 | 0.8611 | 47.1 | 0.2106 | 0.9722 | 75841.93 |
| | | 45 | 0.1405 | 0.8699 | | | | |
| | | 22 | 0.7262 | 0.8373 | | | | |
| | AHA | 18 | 0.6726 | 0.7213 | **11.8** | **0.0899** | **0.9772** | **91328.73** |
| | | 63 | 1.4962 | 0.7827 | | | | |
| | | 58 | 0.8242 | 0.7936 | | | | |

results of the AHA simulation to other algorithms for identifying and sizing numerous RDG units in an IEEE 33 bus system. In comparison to HHO-PSO and PPSOGSA, AHA provides 15.8 KW and 3.7 KW reduced power loss with 2 PV integration, respectively. Furthermore, when compared to HHO-PSO and PPSOGSA, AHA provides 0.8 KW and 3.3 KW reduced power loss with 3 PV integration, accordingly. Furthermore, in contrast with HHO-PSO and PPSOGSA, AHA provides 13.1 KW and 10.6 KW reduced power loss for 2 WT integration, respectively. Moreover, as compared to HHO-PSO and PPSOGSA, AHA provides 29.6 KW and 3.9 KW reduced power loss for 3 WT integration. It is significant to mention that the voltage deviation and VSM values in WT installation scenarios are substantially better due to the reactive power support. Moreover, AHA exceeds the other algorithms in terms of overall yearly energy savings value.

For IEEE 69 bus system, Table 21 compares the results of the AHA simulation to the other methods for locating and sizing several RDG units. In order to reduce power loss and voltage variation, the proposed AHA algorithm appears to outperform the rest of the algorithms studied for the 69-bus system, just as it did for the 33-bus system. In addition, AHA outperforms the other algorithms in terms of yearly energy savings and VSM value. According to the results obtained for both test systems, AHA has the lowest energy loss, lowest voltage deviation, maximum voltage stability margin, and maximum yearly energy savings, which demonstrates the algorithm's superiority over other optimization approaches.

Fig. 4.31 depicts the impact of RDG with optimal placements and sizes on the network voltage

Table 22: Statistics of PPSOGSA, HHO-PSO and AHA

| Case | Method | Best (kW) | Worst (kW) | Mean (kW) | Mean elapsed time (s) |
|---|---|---|---|---|---|
| | HHO-PSO | 70.7 | 76.4 | 72.6 | 10.8 |
| 3 WT | PPSOGSA | 47.1 | 54.2 | 51.4 | 9.7 |
| | AHA | **11.8** | **16.4** | **12.8** | **7.8** |
| | HHO-PSO | 103.6 | 109.6 | 104.7 | 7.4 |
| 3 PV | PPSOGSA | 92.7 | 101.6 | 94.8 | 7.1 |
| | AHA | **91.2** | **93.4** | **92.1** | **5.7** |

profile. The voltage deviation is clearly minimized with proper RDG unit connections, where the voltage magnitude on each bus is within allowed ranges of 0.95-1.05 p.u. Also, it has been identified that AHA provides the optimal solution for each case with the minimum amount of total voltage deviation. Besides, WTs provide a superior voltage profile and significantly improve the system voltage stability compared to PVs because of their ability to supply reactive power. As illustrated in Fig.4.32 , AHA converges significantly faster than HHO-PSO and PPSOGSA for each of the systems. The findings reveal that the AHA accelerates to the near optimal solution swiftly and with consistent convergence characteristics when compared to the other two algorithms. Table 22 compares the best value, worst value and the mean value of the results along with the computational time obtained by PPSOGSA, HHO-PSO, and proposed method over 50 runs in the scenarios of 3 WT and 3 PV installation in IEEE 69 bus system. AHA appears to surpass the other two algorithms in terms of power loss value. In most circumstances, the worst AHA result is better than the best HHO-PSO and PPSOGSA results. Furthermore, AHA outperforms HHO-PSO and PPSOGSA in terms of elapsed time, with HHO-PSO having the longest computing time of all the methods. These statistical indicators strongly suggest that the proposed method outperforms PPSOGSA and HHO-PSO in terms of providing better and more consistent results.

The tested results are obtained using various scenarios in order to demonstrate the algorithm's effectiveness. The suggested technique, known as the Artificial Hummingbird Algorithm, has been found to be more beneficial than previous algorithms for RDG sizing and placement, regardless of whether weather or load uncertainty is included. For added information, the test is completed by considering DGs as dispatchable units ( 2PV, 3 PV, 2WT, 3 WT) for both the IEEE 33 and IEEE 69 bus systems. Furthermore, AHA gives superior solutions and enhances the techno-economic aspects of distribution networks in all the scenarios evaluated.

### 4.3.3 Algorithm parameters variation

The robustness of the AHA algorithm parameters is verified by varying the probability $(0 \sim 1)$ values of the flight and foraging techniques. Fig. 4.33 depicts how the algorithmic parameters affect the power loss values of 3 PV and 3 WT RDG allocation and sizing in a 69 bus test system. The guided foraging technique probability and the diagonal flight probability were adjusted in this

analysis to detect the variance in the results. The findings reveal that modifying the algorithmic parameters has little effect on the $OF_1$ values. According to the findings, the $OF_1$ results had an average standard deviation of 0.247 and 0.513 for 3 WT and 3 PV installments, respectively. Besides, during the simulation, it was also observed that changing the algorithmic parameters slows down the optimization process. As a consequence, it is possible to infer that the algorithmic settings should be kept as default in order to achieve the best results.
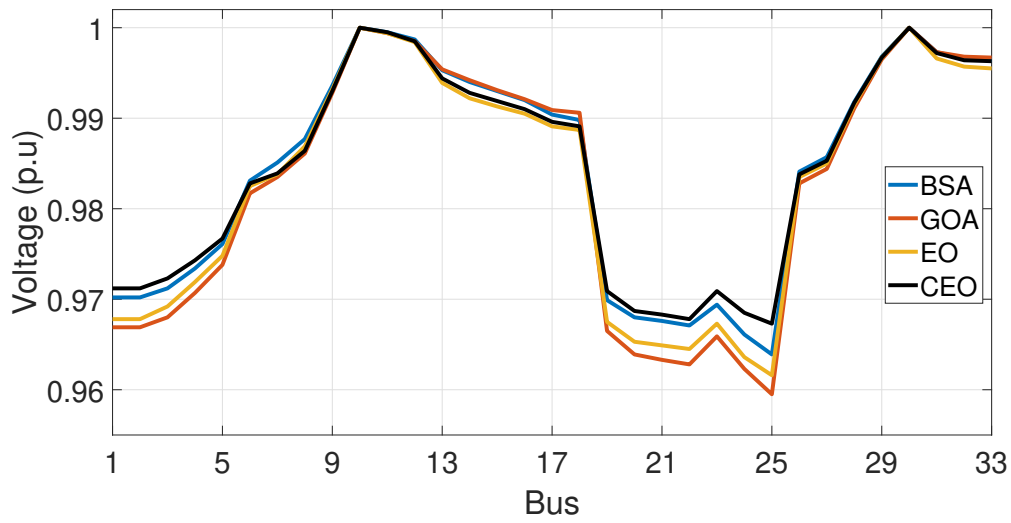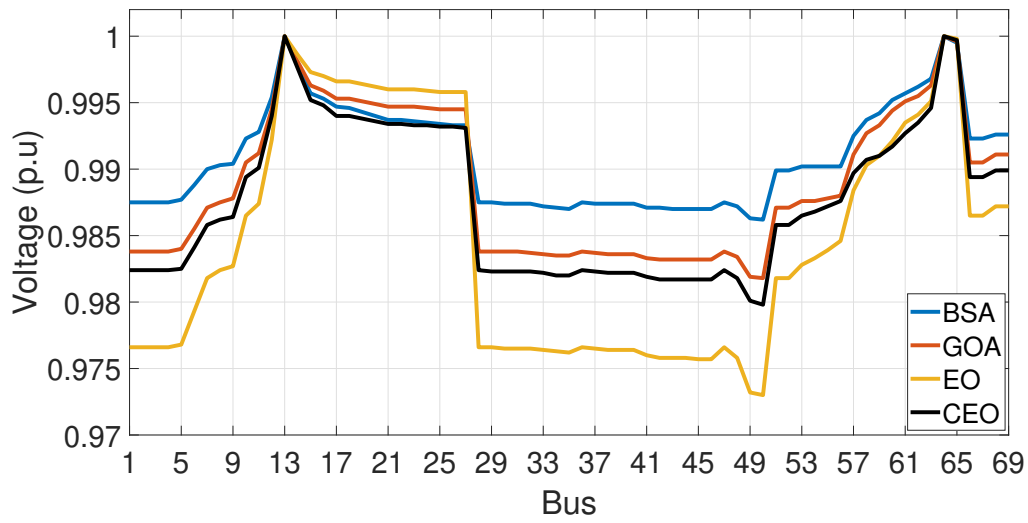
(a) Voltage profile
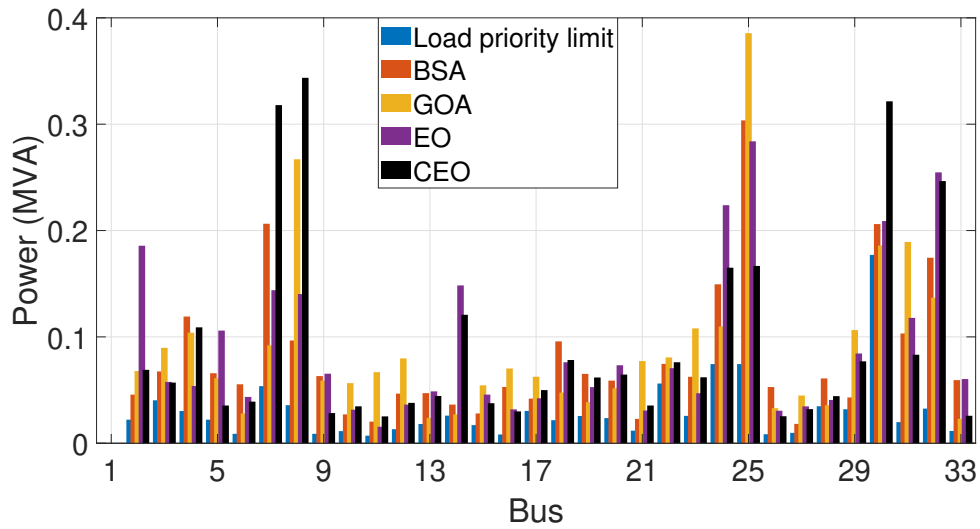


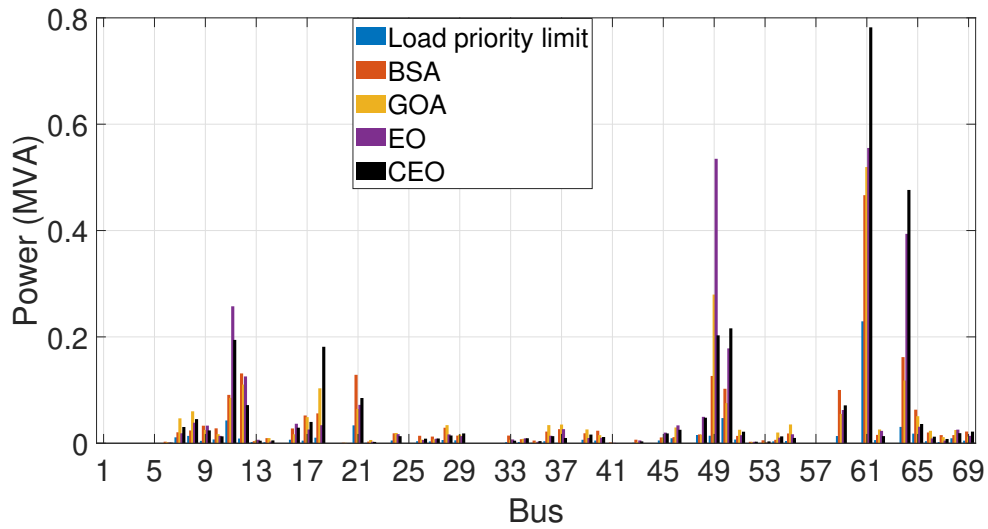(b) Buswise apparent power distribution
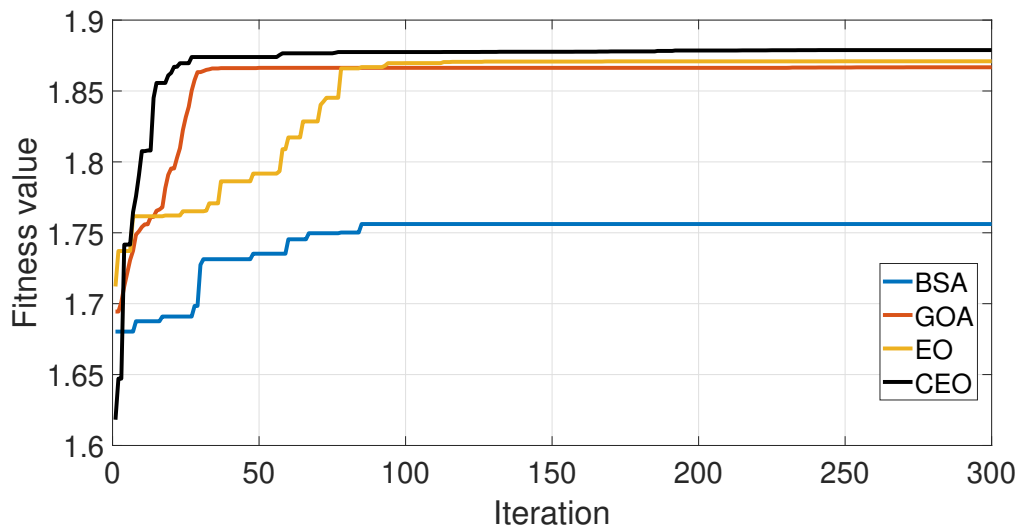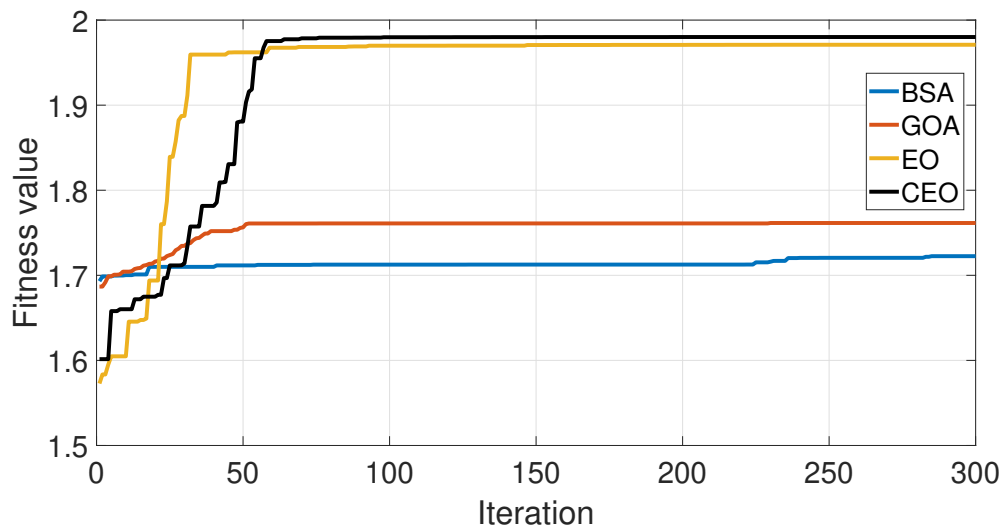


(c) Convergence curve

Figure 4.26: Optimal load shedding results for IEEE 33 bus

(a) Voltage profile



(b) Buswise apparent power distribution



(c) Convergence curve

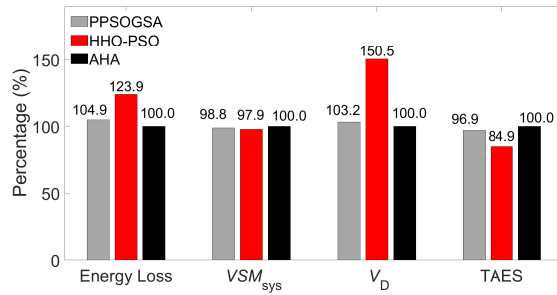Figure 4.27: Optimal load shedding results for IEEE 69 bus

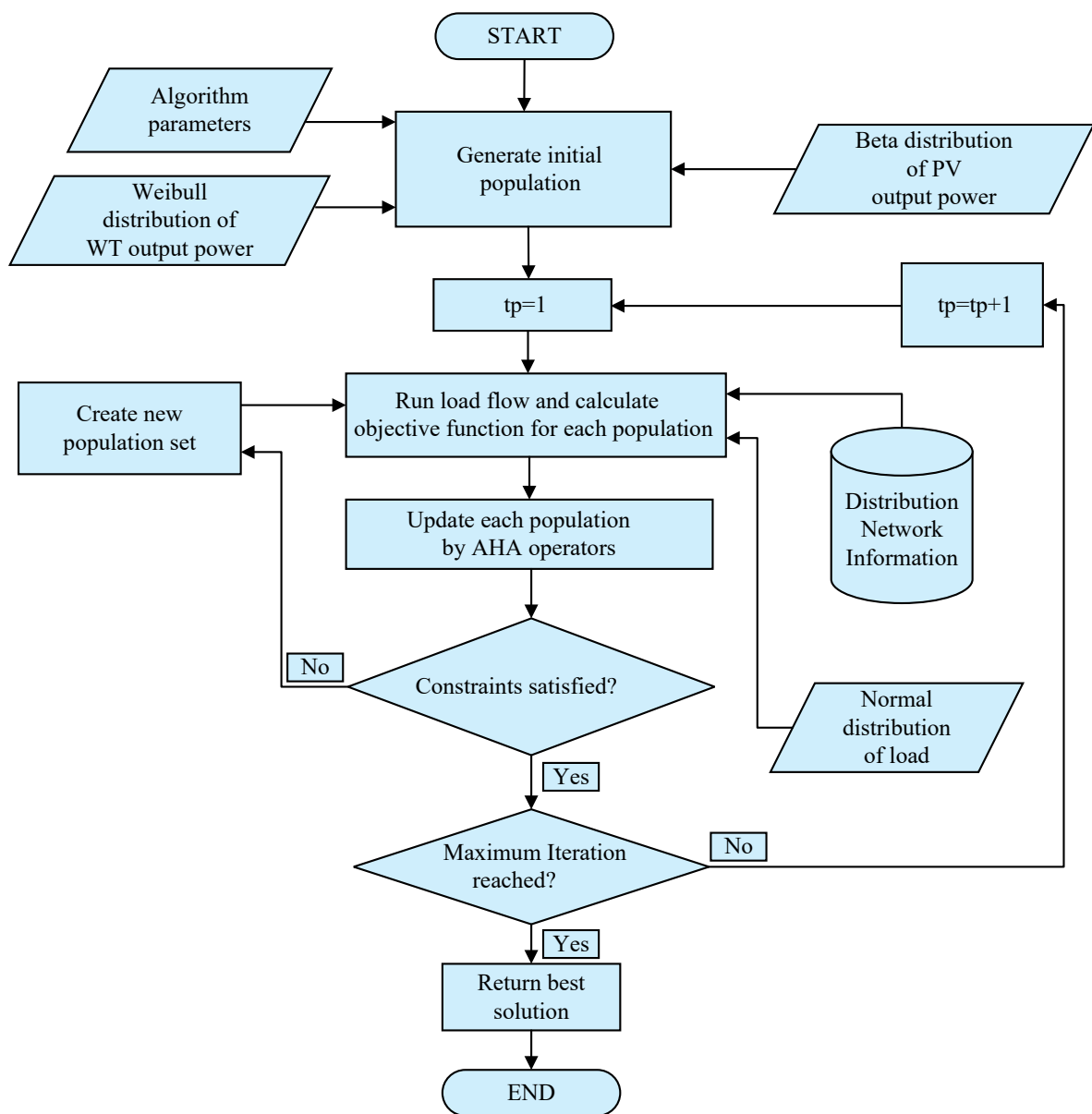Figure 4.28: Optimal results comparison considering uncertainties for IEEE 33 bus (% differences with AHA)



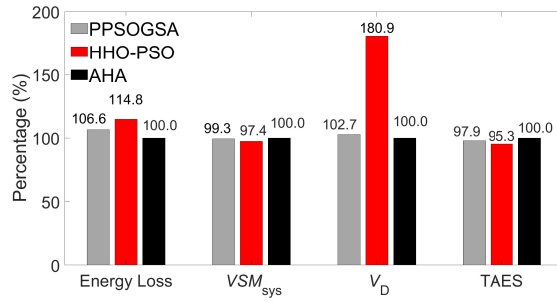Figure 4.29: Flowchart of RDG planning optimization55555
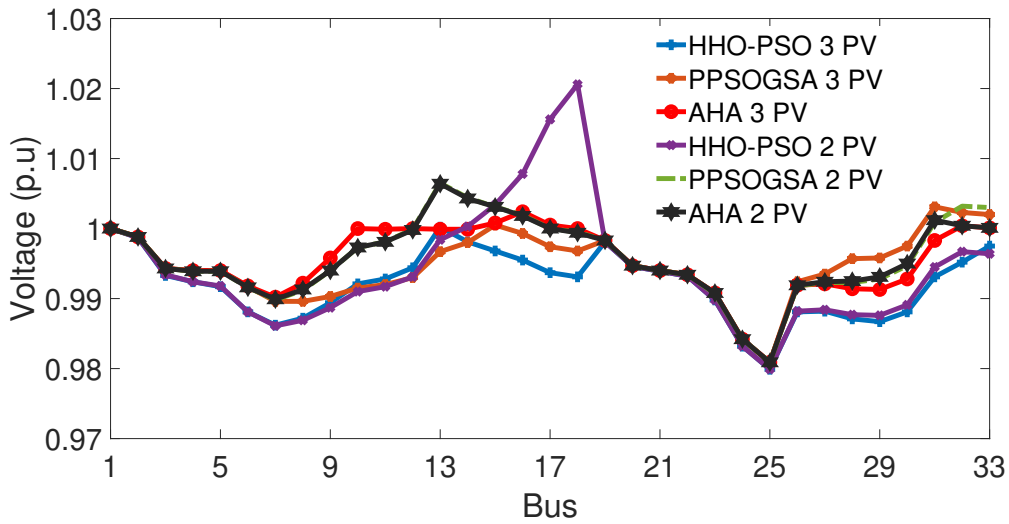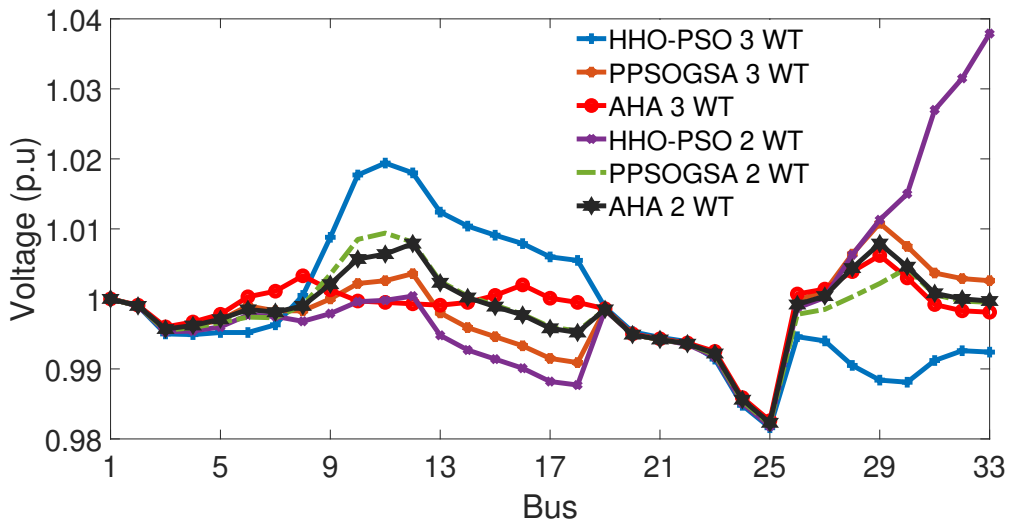
Figure 4.30: Optimal results comparison considering uncertainties for IEEE 69 bus (% differences with AHA)
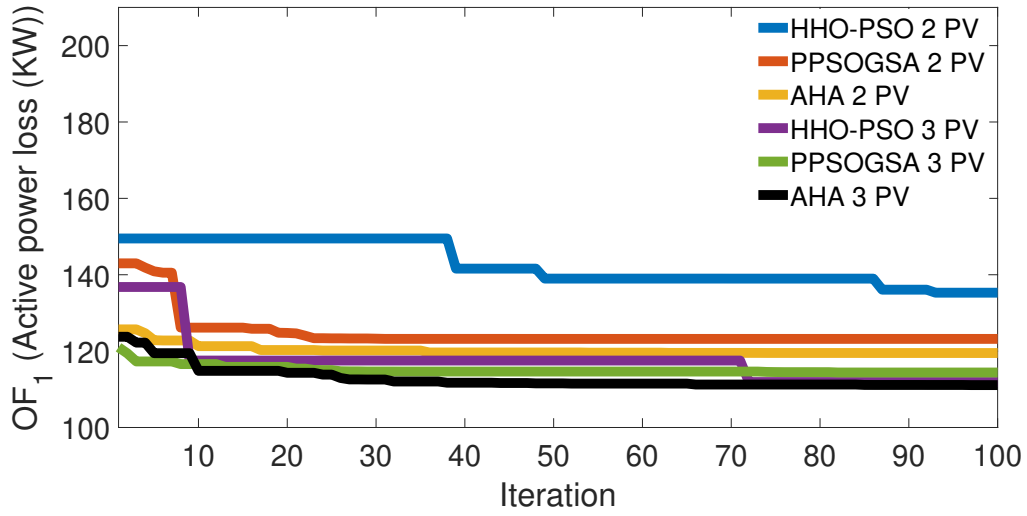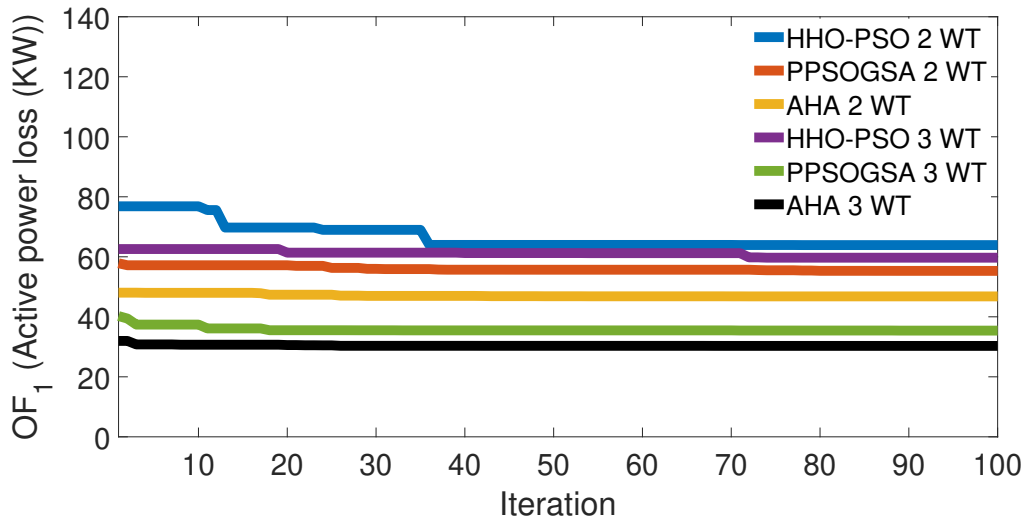


(a) IEEE 33 bus PV unit installation



(b) IEEE 33 bus WT unit installation

Figure 4.31: Voltage profile

(a) IEEE 33 bus PV unit installation



(b) IEEE 33 bus WT unit installation
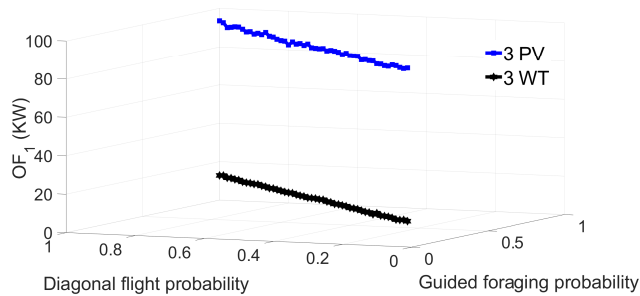
Figure 4.32: Convergence curve



Figure 4.33: AHA algorithmic parameters & $OF_1$

# Chapter 5

## 5 Conclusion

### 5.1 Optimal Load-Shedding in Distribution System

This work provides a novel technique for steady state load shedding optimization in DG integrated islands while considering voltage stability. The objective of attaining appropriate load shedding scheme can be identified by assessing two aspects: total remaining system load and voltage stability margin, $VSM_{sys}$. Obtained results using CSMA have been compared to BSA and SMA in terms mean, standard deviation, best value, worst value, total of elapsed time and convergence of the fitness values. It was observed that CSMA surpasses both BSA and SMA by offering more remaining load and assuring higher voltage stability margin index values. Furthermore, when the network is vast and complicated, CSMA performs significantly better and quicker than BSA and SMA. The advantage of the CSMA approach is that its implementation is simple, with hardly any mathematical complexity, and it provides a better optimum result. Hence, the suggested optimal load shedding scheme can be deployed in a real-world power distribution system that incorporates DGs.

### 5.2 Optimal Sizing and Placement of Multiple DG Units

This work presents a unique approach for optimal DG size and placement in distribution networks, as well as an optimal load shedding technique in DG incorporated islands that considers voltage stability. The optimal DG sizing and placement was determined by minimizing two criteria: voltage deviation and total active power loss. Furthermore, the objective of achieving an effective load shedding scheme was defined by evaluating two criteria: total remaining load and $VSM_{sys}$. In terms of DG placement, CEO results were compared to TLBO, MMFO, and EO in terms of average, standard deviation, best result, worst result, computational speed, and convergence characteristic. Moreover, CEO has been compared to GOA, BSA, and EO for optimal load shedding. According to the findings obtained for DG placement, CEO outperforms all the algorithms by minimizing total active power loss and voltage deviation with better computational speed and early convergence characteristics. Furthermore, in terms of optimal load shedding results, CEO provides higher remaining load and assures greater voltage stability margin values with less computational time and early convergence properties. Therefore, the proposed method can be used in a real-world electrical system.

## 5.3 Optimal Planning of Multiple Renewable Energy-Integrated Distribution System with Uncertainties

This work proposes a novel method for determining the appropriate size and location of RDGs in distribution networks. Four criteria were used to determine the optimal DG size and placement: minimization of voltage deviation, minimization of total active power loss, maximization of voltage stability margin value and maximization of total annual energy savings. The results of the proposed AHA algorithm were compared to those of two recent algorithms, HHO-PSO and PPSOGSA. Two simulation types were considered: with uncertainties and without uncertainties. According to the findings obtained, AHO outperforms all the algorithms for all the objectives with early convergence characteristics for both the simulation types. Therefore, the suggested technique may be recommended for optimal location and sizing of RDGs in real distribution systems considering both weather and load uncertainties. The implications of concurrent installation of PV and WT on existing distribution networks may be studied in the future using real-time load and weather data. Besides, the weighted factors of the techno-economic indices of the objective function can be modified to assess the results variation of the suggested techniques. Moreover, future works may include energy storage technologies for distribution systems.

# References

[1] H. Bevrani, A. G. Tikdari, T. Hiyama., 2010. Power system load shedding: Key issues and new perspectives. World Academy of Science, Engineering and Technology; vol. 65, pp. 199-204, May 2010

[2] Larik, R., Mustafa, M. and Aman, M., 2019. A critical review of the state-of-art schemes for under voltage load shedding. International Transactions on Electrical Energy Systems, 29(5), p.e2828.

[3] Hsu, C., Kang, M. and Chen, C., 2005. Design of adaptive load shedding by artificial neural networks. IEE Proceedings - Generation, Transmission and Distribution, 152(3), p.415.

[4] J. Zhang, C. Lu, C. Fang, X. Ling and Y. Zhang, "Load Shedding Scheme with Deep Reinforcement Learning to Improve Short-term Voltage Stability," 2018 IEEE Innovative Smart Grid Technologies - Asia (ISGT Asia), 2018, pp. 13-18, doi: 10.1109/ISGT-Asia.2018.8467877.

[5] Małkowski, R. and Nieznański, J., 2020. Underfrequency Load Shedding: An Innovative Algorithm Based on Fuzzy Logic. Energies, 13(6), p.1456.

[6] J. Sasikala, M. Ramaswamy, Fuzzy based load shedding strategies for avoiding voltage collapse, Applied Soft Computing, Volume 11, Issue 3, 2011, Pages 3179-3185, ISSN 1568-4946, https://doi.org/10.1016/j.asoc.2010.12.020.

[7] Olabambo Ifeoluwa Oluwasuji, Obaid Malik, Jie Zhang, and Sarvapali Dyanand Ramchurn. 2018. Algorithms for fair load shedding in developing countries. In Proceedings of the 27th International Joint Conference on Artificial Intelligence (IJCAI'18). AAAI Press, 1590–1596.

[8] Alqunun, K., Guesmi, T. Farah, A. Load shedding optimization for economic operation cost in a microgrid. Electr Eng 102, 779–791 (2020). https://doi.org/10.1007/s00202-019-00909-3

[9] G. S. Grewal, J. W. Konowalec and M. M. Hakim, "Optimization of load-shedding scheme in an integrated process plant," in IEEE Transactions on Industry Applications, vol. 35, no. 4, pp. 959-967, July-Aug. 1999, doi: 10.1109/28.777206.

[10] V. Tamilselvan, T. Jayabarathi, A hybrid method for optimal load shedding and improving voltage stability, Ain Shams Engineering Journal, Volume 7, Issue 1, 2016, Pages 223-232, ISSN 2090-4479, https://doi.org/10.1016/j.asej.2015.11.003.

[11] Malekpour, A. and Seifi, A., 2009. An Optimal Load Shedding Approach for Distribution Networks with DGs Considering Capacity Deficiency Modelling of Bulked Power Supply. Modern Applied Science, 3(5).

[12] Ketabi, A. and Hajiakbari Fini, M., 2017. Adaptive underfrequency load shedding using particle swarm optimization algorithm. Journal of Applied Research and Technology, 15(1), pp.54-60.

[13] Talaat, M., Hatata, A., Alsayyari, A. and Alblawi, A., 2020. A smart load management system based on the grasshopper optimization algorithm using the under-frequency load shedding approach. Energy, 190, p.116423.

[14] Wan Afandie, W., 2016. Comparative Analysis of Bacterial Foraging Optimization Algorithm and Evolutionary Programming for Load Shedding in Power System. International Journal of Simulation: Systems, Science Technology,.

[15] Arya, L., Singh, P. and Titare, L., 2012. Differential evolution applied for anticipatory load shedding with voltage stability considerations. International Journal of Electrical Power Energy Systems, 42(1), pp.644-652.

[16] V. G. Calderaro, V.;Lattarrulo,V.;Siano,P.;, "A new algorithm for steady state load-shedding strategy," in 2010, 12th International Conference on Optimization of Electrical and Electronic Equipment (OPTIM) Basov, 2010, p. 48.

[17] Usman, M., Amin, A., Azam, M.M., Mokhlis, H., 2018. Optimal under voltage load shedding scheme for a distribution network using EPSO algorithm, in: 2018 1st International Conference on Power, Energy and Smart Grid (ICPESG). Presented at the 2018 1st International Conference on Power, Energy and Smart Grid (ICPESG), IEEE.

[18] Khamis, A., Shareef, H., Mohamed, A., amp; Dong, Z. Y. (2018). A load shedding scheme for DG integrated islanded power system utilizing backtracking search algorithm. Ain Shams Engineering Journal, 9(1), 161–172. https://doi.org/10.1016/j.asej.2015.10.001

[19] Civicioglu, P., 2013. Backtracking Search Optimization Algorithm for numerical optimization problems. Applied Mathematics and Computation, 219(15), pp.8121-8144.

[20] Acharya, N., Mahat, P. and Mithulananthan, N., 2006. An analytical approach for DG allocation in primary distribution network. International Journal of Electrical Power Energy Systems, 28(10), pp.669-678.

[21] Walling, R., Saint, R., Dugan, R., Burke, J. and Kojovic, L., 2008. Summary of Distributed Resources Impact on Power Delivery Systems. IEEE Transactions on Power Delivery, 23(3), pp.1636-1644.

[22] Xu, Y., Shi, Z., Wang, J. and Hou, P., 2013. Discussion on the Factors Affecting the Stability of Microgrid Based on Distributed Power Supply. Energy and Power Engineering, 05(04), pp.1344-1346.

[23] H. Bevrani, A. G. Tikdari, T. Hiyama., 2010. Power system load shedding: Key issues and new perspectives. World Academy of Science, Engineering and Technology; vol. 65, pp. 199-204, May 2010

[24] Larik, R., Mustafa, M. and Aman, M., 2019. A critical review of the state-of-art schemes for under voltage load shedding. International Transactions on Electrical Energy Systems, 29(5), p.e2828.

[25] P. S. Georgilakis and N. D. Hatziargyriou, "Optimal Distributed Generation Placement in Power Distribution Networks: Models, Methods, and Future Research," in IEEE Transactions on Power Systems, vol. 28, no. 3, pp. 3420-3428, Aug. 2013, doi: 10.1109/TPWRS.2012.2237043.

[26] Kansal, Satish Kumar, Vishal. (2013). Optimal placement of different type of DG sources in distribution networks. International Journal of Electrical Power Energy Systems. 53. 752–760. 10.1016/j.ijepes.2013.05.040.

[27] R. Sanjay, T. Jayabarathi, T. Raghunathan, V. Ramesh and N. Mithulananthan, "Optimal Allocation of Distributed Generation Using Hybrid Grey Wolf Optimizer," in IEEE Access, vol. 5, pp. 14807-14818, 2017, doi: 10.1109/ACCESS.2017.2726586.

[28] Samala, R.K., Kotapuri, M.R. Optimal allocation of distributed generations using hybrid technique with fuzzy logic controller radial distribution system. SN Appl. Sci. 2, 191 (2020). https://doi.org/10.1007/s42452-020-1957-3

[29] Kumar, S., Mandal, K. and Chakraborty, N., 2019. Optimal DG placement by multi-objective opposition based chaotic differential evolution for techno-economic analysis. Applied Soft Computing, 78, pp.70-83.

[30] Elattar, E. and Elsayed, S., 2020. Optimal Location and Sizing of Distributed Generators Based on Renewable Energy Sources Using Modified Moth Flame Optimization Technique. IEEE Access, 8, pp.109625-109638.

[31] Vita, V., 2017. Development of a Decision-Making Algorithm for the Optimum Size and Placement of Distributed Generation Units in Distribution Networks. Energies, 10(9), p.1433.

[32] Rani, B. and Reddy, A., 2019. Optimal Allocation and Sizing of Multiple DG in Radial Distribution System Using Binary Particle Swarm Optimization. International Journal of Intelligent Engineering and Systems, 12(1), pp.290-299.

[33] Memarzadeh G, Keynia F. A new index-based method for optimal DG placement in distribution networks. Engineering Reports. 2020;e12243. https://doi.org/10.1002/eng2.12243

[34] M.C.V. Suresh, J. Belwin Edward,A hybrid algorithm based optimal placement of DG units for loss reduction in the distribution system, Applied Soft Computing,Volume 91,2020,106191,ISSN 1568-4946, https://doi.org/10.1016/j.asoc.2020.106191.

[35] Hassan, A., Sun, Y. and Wang, Z., 2020. Multi-objective for optimal placement and sizing DG units in reducing loss of power and enhancing voltage profile using BPSO-SLFA. Energy Reports, 6, pp.1581-1589.

[36] A. Selim, S. Kamel, A. S. Alghamdi and F. Jurado, "Optimal Placement of DGs in Distribution System Using an Improved Harris Hawks Optimizer Based on Single- and Multi-Objective Approaches," in IEEE Access, vol. 8, pp. 52815-52829, 2020, doi: 10.1109/ACCESS.2020.2980245.

[37] Talaat, M., Hatata, A., Alsayyari, A. and Alblawi, A., 2020. A smart load management system based on the grasshopper optimization algorithm using the under-frequency load shedding approach. Energy, 190, p.116423.

[38] Khamis, A., Shareef, H., Mohamed, A., amp; Dong, Z. Y. (2018). A load shedding scheme for DG integrated islanded power system utilizing backtracking search algorithm. Ain Shams Engineering Journal, 9(1), 161–172. https://doi.org/10.1016/j.asej.2015.10.001

[39] Arya, L., Singh, P. and Titare, L., 2012. Differential evolution applied for anticipatory load shedding with voltage stability considerations. International Journal of Electrical Power Energy Systems, 42(1), pp.644-652.

[40] Wan Afandie, W., 2016. Comparative Analysis of Bacterial Foraging Optimization Algorithm and Evolutionary Programming for Load Shedding in Power System. International Journal of Simulation: Systems, Science  Technology,.

[41] V. G. Calderaro, V.;Lattarrulo,V.;Siano,P.;, "A new algorithm for steady state load-shedding strategy," in 2010, 12th International Conference on Optimization of Electrical and Electronic Equipment (OPTIM) Basov, 2010, p. 48.

[42] Usman, M., Amin, A., Azam, M.M., Mokhlis, H., 2018. Optimal under voltage load shedding scheme for a distribution network using EPSO algorithm, in: 2018 1st International Conference on Power, Energy and Smart Grid (ICPESG). Presented at the 2018 1st International Conference on Power, Energy and Smart Grid (ICPESG), IEEE.

[43] Mohanty, B. and Tripathy, S., 2016. A teaching learning based optimization technique for optimal location and size of DG in distribution network. Journal of Electrical Systems and Information Technology, 3(1), pp.33-44.

[44] Khamis, A., Shareef, H. and Mohamed, A., 2015. Islanding detection and load shedding scheme for radial distribution systems integrated with dispersed generations. IET Generation, Transmission Distribution, 9(15), pp.2261-2275.

[45] VK Mehta & Rohit Mehta (2005). *Principles of Power System: Including Generation, Transmission, Distribution, Switchgear and Protection: for BE/B. Tech., AMIE and Other Engineering Examinations.* S. Chand Publishing.

[46] Lopes, João Abel Peças et al. "Integrating distributed generation into electric power systems: A review of drivers, challenges and opportunities." *Electric Power Systems Research*, 77 (2007): 1189-1203.

[47] Omar Ellabban, Haitham Abu-Rub and Frede Blaabjerg. "Renewable Energy Resources: Current status, future prospects and their enabling technology." *Renewable and Sustainable Energy Reviews*, 39 (2014), 748–764.

[48] Stefan Weitemeyer, David Kleinhans et al. "Integration of renewable energy sources in future power systems: The role of Storage." *Renewable Energy*, 75 (2015), 14–20.

[49] M. Liserre, T. Sauter and J. Y. Hung. "Future Energy Systems: Integrating Renewable Energy Sources into the Smart Power Grid Through Industrial Electronics", in *IEEE Industrial Electronics Magazine*, vol. 4, no. 1, pp. 18-37, March 2010.

[50] Falkoni, Anamarija Krajacic, Goran Puksec, Tomislav Duic, Neven (2015). The integration of renewable energy sources and electric vehicles into the power system of the Dubrovnik region. *Energy, Sustainability and Society*, 5(1).

[51] Dudiak, Jozef and Michal Kolcun. "Integration of renewable energy sources to the power system." *2014 14th International Conference on Environment and Electrical Engineering* (2014): 148-151.

[52] Paliwal, Priyanka Patidar, N.P. & Nema, R.K., 2014. "Planning of grid integrated distributed generators: A review of technology, objectives and techniques," *Renewable and Sustainable Energy Reviews*, Elsevier, vol. 40(C), pages 557-570.

[53] Ndamulelo Mararakanye, Bernard Bekker (2019). "Renewable energy integration impacts within the context of generator type, penetration level and grid characteristics." Renewable and Sustainable Energy Reviews, 108, 441–451.

[54] Grant Allan, Igor Eromenko, Michelle Gilmartin, Ivana Kockar, Peter McGregor (2015). "The economics of Distributed Energy Generation: A Literature Review." Renewable and Sustainable Energy Reviews, 42, 543–556.

[55] Mudathir Funsho Akorede, Hashim Hizam, Edris Pouresmaeil (2010). "Distributed Energy Resources and benefits to the environment." Renewable and Sustainable Energy Reviews, 14(2), 724–734.

[56] Zubo, R. H. A., Mokryani, G., Rajamani, H.-S., Aghaei, J., Niknam, T., amp; Pillai, P. (2017). "Operation and planning of distribution networks with integration of renewable distributed generators considering uncertainties: A Review." Renewable and Sustainable Energy Reviews, 72, 1177–1198.

[57] Esmaeili, S.; Anvari-Moghaddam, A.; Jadid, S. Optimal Operational Scheduling of Reconfigurable Multi-Microgrids Considering Energy Storage Systems. Energies 2019, 12, 1766.

[58] Najafi, J., Peiravi, A., Anvari-Moghaddam, A., Guerrero, J. M. (2019). "Resilience Improvement Planning of power-water distribution systems with multiple microgrids against hurricanes using clean strategies." *Journal of Cleaner Production*, 223, 109–126.

[59] Hassan, A. S., Othman, E. S. A., Bendary, F. M., amp; Ebrahim, M. A. (2020). "Optimal integration of distributed generation resources in active distribution networks for techno-economic benefits." *Energy Reports*, 6, 3462–3471.

[60] Jordehi, A. R. (2018). "How to deal with uncertainties in Electric Power Systems? A Review." *Renewable and Sustainable Energy Reviews*, 96, 145–155.

[61] Soroudi, A., Aien, M., amp; Ehsan, M. (2012)." A probabilistic modeling of photo voltaic modules and wind power generation impact on distribution networks." *IEEE Systems Journal*, 6(2), 254–259.

[62] Maleki, A., Khajeh, M. G., Ameri, M. (2016). "Optimal sizing of a grid independent hybrid renewable energy system incorporating resource uncertainty, and load uncertainty." *International Journal of Electrical Power and Energy Systems*, 83, 514–524.

[63] Elkadeem, M. R., Abd Elaziz, M., Ullah, Z., Wang, S., Sharshir, S. W. (2019). "Optimal planning of renewable energy-integrated distribution system considering uncertainties." *IEEE Access*, 7, 164887–164907.

[64] Radosavljevic, J., Arsic, N., Milovanovic, M., amp; Ktena, A. (2020). "Optimal placement and sizing of renewable distributed generation using hybrid metaheuristic algorithm." *Journal of Modern Power Systems and Clean Energy*, 8(3), 499–510.

[65] Ali, E. S., Abd Elazim, S. M., amp; Abdelaziz, A. Y. (2016). "Optimal allocation and sizing of renewable distributed generation using Ant Lion Optimization algorithm." *Electrical Engineering*, 100(1), 99–109.

[66] El-Fergany, A. (2015). "Optimal allocation of multi-type distributed generators using backtracking search optimization algorithm." *International Journal of Electrical Power and Energy Systems*, 64, 1197–1205.

[67] Abu-Mouti, F. S., amp; El-Hawary, M. E. (2009). "Modified artificial bee colony algorithm for optimal distributed generation sizing and allocation in distribution systems." 2009 *IEEE Electrical Power and Energy Conference* (EPEC).

[68] Sanjay, R., Jayabarathi, T., Raghunathan, T., Ramesh, V., Mithulananthan, N. (2017). "Optimal allocation of distributed generation using Hybrid Grey Wolf optimizer." *IEEE Access*, 5, 14807–14818.

[69] Mohamed Imran A, amp; Kowsalya M. (2014). "Optimal size and siting of multiple distributed generators in distribution system using bacterial foraging optimization." *Swarm and Evolutionary Computation*, 15, 58–65.

[70] Rama Prabha, D., Jayabarathi, T., Umamageswari, R., Saranya, S. (2015). "Optimal allocation and sizing of distributed generation unit using Intelligent Water Drop algorithm." *Sustainable Energy Technologies and Assessments*, 11, 106–113.

[71] ChithraDevi, S. A., Lakshminarasimman, L., amp; Balamurugan, R. (2017). "Stud krill herd algorithm for multiple DG placement and sizing in a radial distribution system." *Engineering Science and Technology, an International Journal*, 20(2), 748–759.

[72] Moradi, M. H., amp; Abedini, M. (2012). "A combination of genetic algorithm and particle swarm optimization for optimal distributed generation location and sizing in distribution systems with fuzzy optimal theory." *International Journal of Green Energy*, 9(7), 641–660.

[73] Kaur, S., Kumbhar, G., Sharma, J. (2014). "A MINLP technique for optimal placement of multiple DG units in Distribution Systems." *International Journal of Electrical Power and Energy Systems*, 63, 609–617.

[74] Kumar, S., Mandal, K. K., Chakraborty, N. (2019). "Optimal DG placement by multi-objective opposition based chaotic differential evolution for techno-economic analysis." *Applied Soft Computing*, 78, 70–83.

[75] Khatod, D. K., Pant, V., Sharma, J. (2013). "Evolutionary programming based optimal placement of renewable distributed generators." *IEEE Transactions on Power Systems*, 28(2), 683–695.

[76] Abdelaziz, A. Y., Hegazy, Y. G., El-Khattam, W., Othman, M. M. (2015). "Optimal allocation of stochastically dependent renewable energy based distributed generators in unbalanced distribution networks." *Electric Power Systems Research*, 119, 34–44.

[77] Kayal, P., Chanda, C. K. (2015). "Optimal mix of solar and wind distributed generations considering performance improvement of Electrical Distribution Network." *Renewable Energy*, 75, 173–186.

[78] Ali, Abdelfatah  Mahmoud, Karar  Lehtonen, Matti. (2021). "Optimal planning of inverter-based renewable energy sources towards autonomous microgrids accommodating electric vehicle charging stations." *IET Generation, Transmission and Distribution.* 16.

[79] A. Ali, K. Mahmoud and M. Lehtonen. "Optimization of Photovoltaic and Wind Generation Systems for Autonomous Microgrids With PEV-Parking Lots." *IEEE Systems Journal.*

[80] Biswal, S. R., Shankar, G., Elavarasan, R. M.,  Mihet-Popa, L. (2021). "Optimal allocation/sizing of dgs/capacitors in reconfigured radial distribution system using quasi-reflected slime mould algorithm." *IEEE Access*, 9, 125658–125677.

[81] Zellagui, M., Belbachir, N.,  Ziad El-Bayeh, C. (2021). "Optimal allocation of RDG in distribution system considering the seasonal uncertainties of load demand and solar-wind

generation systems." *IEEE EUROCON 2021 - 19th International Conference on Smart Technologies*.

[82] Lekvan, A. A., Habibifar, R., Moradi, M., Khoshjahan, M., Nojavan, S., & Jermsittiparsert, K. (2021). "Robust optimization of renewable-based multi-energy micro-grid integrated with flexible energy conversion and storage devices." *Sustainable Cities and Society*, 64, 102532.

[83] Galvani, S., Bagheri, A., Farhadi-Kangarlu, M., & Nikdel, N. (2022). "A multi-objective probabilistic approach for smart voltage control in wind-energy integrated networks considering correlated parameters." *Sustainable Cities and Society*, 78, 103651.

[84] Geng, J., Zheng, T., Cao, J., Yang, Y., Jin, Y., Fu, J. (2022). "Research on multi-objective Operation Optimization of Multi Energy Integrated Service stations based on Autonomous Collaborative Control." *Energy Reports*, 8, 278–284.

[85] Dinakara P et al (2018)." Optimal renewable resources placement in distribution networks by Combined Power Loss Index and whale optimization algorithms." *Journal of Electrical Systems and Information Technology*, 5(2), 175–191.

[86] Tolba, M., Rezk, H., Tulsky, V., Diab, A., Abdelaziz, A., Vanin, A. (2018). "Impact of optimum allocation of renewable distributed generations on distribution networks based on different optimization algorithms." *Energies*, 11(1), 245.

[87] Nawaz, S., Bansal, D. A. K., Sharma, D. M. (2017). "A novel approach for multiple DG allocation in real distribution system." *International Journal of Engineering and Technology*, 9(2), 963–968.

[88] El-Fergany, A. (2015). "Multi-objective allocation of multi-type distributed generators along distribution networks using backtracking search algorithm and Fuzzy Expert Rules." *Electric Power Components and Systems*, 44(3), 252–267.

[89] Biswas, P. P., Suganthan, P. N., Mallipeddi, R., Amaratunga, G. A. J. (2019). "Optimal reactive power dispatch with uncertainties in load demand and renewable energy sources adopting scenario-based approach." *Applied Soft Computing*, 75, 616–632.

[90] Li, S., Chen, H., Wang, M., Heidari, A. and Mirjalili, S., 2020. Slime mould algorithm: A new method for stochastic optimization. Future Generation Computer Systems, 111, pp.300-323.

[91] A. Faramarzi, M. Heidarinejad, B. Stephens et al., Equilibrium optimizer:A novel optimization algorithm, Knowledge-Based Systems (2019), doi:https://doi.org/10.1016/j.knosys.2019.105190

[92] Zhao, W., Wang, L., amp; Mirjalili, S. (2022). "Artificial Hummingbird Algorithm: A new bio-inspired optimizer with its engineering applications." *Computer Methods in Applied Mechanics and Engineering*, 388, 114194.

[93] M. H. Hauqe, "A linear static voltage stability margin for radial distribution systems," 2006 IEEE Power Engineering Society General Meeting, 2006, pp. 6 pp.-, doi: 10.1109/PES.2006.1708954.

[94] Open data sets. "IEEE PES Intelligent Systems Subcommittee". Available: `https://site.ieee.org/pes-iss/data-sets/` (accessed Feb. 3, 2022).

[95] Power Systems Test Case Archive. "Reliability test system". Available :`http://labs.ece.uw.edu/pstca/rts/pg_tcarts.htm` (accessed Feb. 3, 2022).